The Seasonal Phases of an Arctic Lagoon Reveal the Discontinuities of pH Variability and CO_2 Flux at the Air-sea Interface

Cale A. Miller[1,3], Christina Bonsell[2], Nathan D. McTigue[2], Amanda L. Kelley[3]

[1] Department of Evolution and Ecology, University of California Davis, Davis, CA, USA, 95616
[2] Marine Science Institute, The University of Texas at Austin, Port Aransas, TX, USA, 78373
[3] College of Fisheries and Ocean Sciences, University of Alaska Fairbanks, Fairbanks, AK, USA, 99775

Correspondence to: Cale A. Miller (cmill@ucdavis.edu; calemiller620@gmail.com)

Abstract

The western Arctic Ocean, including its shelves and coastal habitats, has become a focus in ocean acidification research over the past decade as the colder waters of the region and the reduction of sea ice appear to promote the uptake of excess atmospheric CO_2. Due to seasonal sea ice coverage, high-frequency monitoring of pH or other carbonate chemistry parameters is typically limited to infrequent ship-based transects during ice-free summers. This approach has failed to capture year-round nearshore carbonate chemistry dynamics which is modulated by biological metabolism in response to abundant allochthonous organic matter to the narrow shelf of the Beaufort Sea and adjacent regions. The coastline of the Beaufort Sea comprises a series of lagoons that account for > 50 % of the land-sea interface. The lagoon ecosystems are novel features that cycle between "open" and "closed" phases (i.e., ice-free, and ice-covered, respectively). In this study, we collected high-frequency pH, salinity, temperature, and PAR measurements in association with the Beaufort Lagoon Ecosystems—Long Term Ecological Research—for an entire calendar year in Kaktovik Lagoon, Alaska, USA, capturing two open water phases and one closed phase. Hourly pH variability during the open water phases are some of the fastest rates reported, exceeding 0.4 units. Baseline pH varied substantially between open phase 2018 and open phase 2019 from ~ 7.85 to 8.05, respectively, despite similar hourly rates of change. Salinity-pH relationships were mixed during all three phases displaying no correlation in open 2018, a negative correlation in closed 2018 – 2019, and positive correlation during open 2019. The high-frequency of pH variability could partially be explained by photosynthesis-respiration cycles as correlation coefficients between daily average pH and PAR were 0.46 and 0.64 for open 2018 and open 2019 phases, respectively. The estimated annual daily average CO_2 efflux (from sea to atmosphere) was 5.9 ± 19.3 mmol m^{-2} d^{-1}, which is converse to the negative

influx of CO_2 estimated for the coastal Beaufort Sea despite exhibiting extreme variability. Considering the geomorphic differences such as depth and enclosure in Beaufort Sea lagoons, further investigation is needed to assess if there are periods of the open phase in which all lagoons are sources of carbon to the atmosphere, potentially offsetting the predicted sink capacity of the greater Beaufort Sea.

1 Introduction

Acidification of the Arctic Ocean is predicted to proceed at a faster rate than lower latitude regions due to the increased solubility of CO_2 in colder waters, intrinsically lower carbonate ion concentration, and specific water mass mixing patterns with deep Pacific water and surface freshwater (Fabry et al., 2009; Mathis et al., 2015). The acidification phenomenon which increases the dissolved inorganic carbon to alkalinity ratio reduces the natural buffering capacity of the carbonate system via a reduction in carbonate ion concentration. These processes result in a decrease of calcium carbonate saturation state and sea surface pH. It is estimated that the Canadian Basin, Beaufort Sea, and Chukchi Sea in the Arctic have experienced a 2.7 % shoaling of low aragonite saturation state ($\Omega_{arg} < 1.25$) waters from 0 – 250 m over the past 2 decades (Qi et al., 2017; Zhang et al., 2020). Future projections anticipate a continuation of this trend with sustained, perennial, undersaturation of calcium carbonate ($\Omega_{arg} < 1$) in the Beaufort and Chukchi Seas by the year 2040, which will reduce the capacity of these waters to continually take up atmospheric CO_2 (Mathis et al., 2015). The rate at which this happens will have significant implications on the current estimates of CO_2 uptake by the coastal Chukchi and Beaufort Seas (Evans et al. 2015a). Acidification of offshore Arctic waters appear to be a consequence of increasing Pacific Winter Water intrusion due to globally warming waters and an influx of excess atmospheric CO_2 caused by the disequilibrium between air and seawater PCO_2 (Qi et al., 2017). Along the nearshore regions of the Beaufort Sea, however, coastal processes predominately drive acidification such as riverine flux of freshwater, biological metabolism, sea-ice melt from warming waters, and upwelling of the Polar Marine Layer which is an important water source for Arctic lagoons (Miller et al., 2014; Wynn et al., 2016; Harris et al., 2017; Carstensen and Duarte, 2019; Woosley and Millero, 2020).

125 The coastal margin of the Beaufort Sea consists of biologically complex, shallow (< 6 m),
126 discontinuous, estuarine lagoons that depict ~ 50 % of the coast from Nuvuk (Pt. Barrow) to
127 Demarcation Bay, Alaska, USA (Lissauer et al., 1984; Dunton et al., 2006, 2012; Harris et al.,
128 2017). The North Slope region is predominately tundra, where the annual terrestrial thaw
129 comprises the majority of the freshwater outflow to the Beaufort Sea. Canada's Mackenzie River
130 is the largest source of freshwater flowing into the Beaufort Sea, ~ 300 km^3 yr^{-1} (Stein and
131 Macdonald, 2004; McClelland et al., 2006); however, many smaller rivers and streams link the
132 terrestrial hydrography with the marine lagoon ecosystem characterized as geomorphic transition
133 zones (Dunton et al., 2006, 2012). Barrier islands partially obstruct Beaufort Sea coastal water
134 exchange with the lagoons, which in part are hydrographically influenced by the seasonal shifts
135 in terrestrial freshwater flux that results in highly dynamic chemical conditions (Mouillot et al.,
136 2007). Flow channels between the land, Arctic lagoons and the ocean are ephemeral, causing the
137 flow of water in and out of a lagoon to be intermittent, varying on short- and long-term time
138 scales (Kraus et al., 2008; Dunton et al., 2012). These physical flow attributes result in highly
139 variable salinity and temperature that range from fresh to hypersaline (0 to >45), and -2 ˚C to 14
140 ˚C, respectively (Dunton and Schonberg, 2006; Harris et al., 2017). This variability in
141 temperature and freshwater delivery can have a dramatic effect on carbonate chemistry
142 thermodynamics and modify alkalinity and dissolved inorganic carbon (DIC). The seasonality of
143 these shallow lagoons is distinguished by two principal phase states corresponding to sea ice
144 prevalence—open and closed. The closed period during winter ice cover exhibits a non-
145 quantifiable amount of air-sea exchange due to the physical sea ice barrier. Conversely, the open,
146 ice-free summer period from late spring to early fall is marked by spring river discharge, air-sea
147 exchanges, and storm activity (McClelland et al., 2012, 2014). Episodic fluctuations in lagoon

148 hydrography during periods of open water add to the complexity of physicochemical variability
149 as wind-driven upwelling events coupled with tidal flux can precipitate rapid changes in these
150 semi-isolated bodies of water (Lissauer et al., 1984).

151 Despite extreme variability in temperature and salinity, Arctic lagoons are home to
152 diverse fish assemblages that include diadromous, freshwater, and marine species (Robards,
153 2014; Harris et al., 2017; Tibbles, 2018), many of which serve as important subsistence fisheries
154 for Arctic communities (Griffiths et al., 1977; Craig, 1989). Arctic lagoons have relatively high
155 diversity and abundance of benthic community invertebrates, ranging from 654 to 5,353
156 individuals m^{-2} with trophic linkages to birds and marine mammals (Griffiths et al., 1977,
157 Johnson et al., 2010; Dunton et al., 2012). The benthic food web relies on both autochthonous
158 microalgal production and allochthonous terrestrial organic matter (OM) inputs as carbon
159 subsidies (Harris et al., 2018). The deposition of these carbon subsidies may have implications
160 on the chemical conditions of lagoon ecosystems via enhanced remineralization during the
161 during open and closed phases. To date, hydrographic physicochemical measurements have been
162 mostly limited to the open [summer] season with few exceptions (Kinney et al., 1971; Mathews
163 and Stringer, 1984; Dunton and Schonberg, 2006; Robards, 2014). To our knowledge, only a
164 single high-frequency year-round measurement of Beaufort Sea lagoon temperature and salinity
165 exists (Harris et al., 2017), which is insufficient for understanding how these factors including
166 biological metabolism may impact carbonate system dynamics.

167 This study is the first to incorporate a high-frequency time series of salinity, temperature,
168 PAR, and pH for an entire calendar year capturing both open and closed phases of an Arctic
169 lagoon. The Kaktovik Lagoon located adjacent to Barter Island and the city of Kaktovik was
170 selected for sensor package deployment. The data collected in this study were processed in part

171 with those available from the Beaufort Lagoon Ecosystems (BLE) Long Term Ecological
172 Research Program (LTER) and the NOAA Earth Systems Research Laboratory (ESRL). Salinity,
173 temperature, and pH were analyzed in the time and frequency domains alongside ancillary solar
174 radiation and water depth in order to examine potential modifiers of pH. This included estimates
175 of carbon flux at the land-sea interface utilizing atmospheric PCO_2 measurements and comparing
176 those with derived seawater PCO_2 estimates. The findings of this study are presented in the
177 context of seasonal variability of oceanographic processes in an ecosystem that is part of the
178 western coastal Arctic that is experiencing climate change.
179

180 ## 2 Study site and methods

181 ### 2.1 Kaktovik Lagoon ecosystem

182 Kaktovik Lagoon, Alaska (70° 6' 3" N 143° 34' 52" W), serves as one of the study sites for the
183 National Science Foundation's Beaufort Lagoon Ecosystems LTER. It is one of a series of
184 coastal lagoons that fringe the Arctic National Wildlife Refuge and borders the east side of
185 Barter Island. With a maximum depth of approximately 4.4 m, Kaktovik Lagoon has two narrow
186 exchange pathways with adjacent water bodies (Dunton et al., 2012). One of the pathways
187 connects to Arey Lagoon, the other links to Jago Lagoon and to the Beaufort Sea via a channel >
188 25 m long and < 2.5 m deep (Fig. 1). Surface freshwater inputs are limited to small tundra
189 streams, although narrow inlets provide some exchange to adjacent Arey and Jago Lagoons,
190 which receive terrestrial inputs from the Hulahula/Okpilak and Jago Rivers, respectively. The
191 timing of sea ice formation varies by year but occurs between late September and October
192 becoming landfast (fastened to the coastline) in the shallow lagoons until breakup in May or June
193 (Dunton et al., 2006).

2.2 Oceanographic sampling

A benthic mooring outfitted with a SeaBird SeaFET V2 and RBR Concerto CTD++ was deployed 8 August 2018 to 11 August 2019, with sensors roughly 10 cm from the bottom in Kaktovik Lagoon (Fig. 1). Hourly measurements of pH, salinity, and temperature (from SeaFET thermistor) were recorded (UTC) throughout the deployment period. A separate, adjacent mooring consisting of a LI-COR spherical quantum sensor in-line with a LI-1000 datalogger recorded photosynthetically active radiation (PAR μmol photons m^{-2} s^{-1}; 400-700 nm) ~ 30 cm from the bottom. Average PAR was integrated over three-hour time periods and recorded. In August 2018, April 2019, and June 2019, the site was sampled for dissolved nutrients and physicochemical (i.e., temperature and conductivity) parameters within 30 cm of water surface and within 30 cm of the bottom. Physicochemical parameters were recorded with a YSI ProDSS calibrated daily before excursions. Nutrient samples were collected with a peristaltic pump fitted with Masterflex C-flex tubing, then filtered through a Geotech 0.45 μm high-capacity polyethersulfone (PES) capsule filter connected with Masterflex-C tubing and frozen at -20 ˚C until analysis. Sediment was retrieved from the seafloor by a 0.1 m^2 van Veen grab, sampled with 50 mL push core and frozen at -20 ˚C until analysis. Porewater was extracted by centrifugation of defrosted sediment, then analyzed immediately. Dissolved nutrients in water and porewater [ammonia (NH_3), nitrate + nitrite (NO_x), orthophosphate (PO_4^{3-}), and silica (SiO_2)] were measured at the Core Facilities Laboratory at The University of Texas Marine Science Institute in Port Aransas, Texas, on a continuous flow-analyzer Lachat Quick Chem 8500.

2.3 Seawater chemistry and pH sensor calibration

Discrete bottle samples were taken approximately 10 cm off the bottom proximal to the sensor on 17 August 2018 for SeaFET calibration, and 26 April 2019 for reference. Bottle samples were collected in duplicate and processed for total alkalinity (A_T) and pH_T (total scale). An additional A_T sample was collected on 21 June 2019. The August 2018 sample was gathered by Van Dorn bottle, where a single sampling was used to fill duplicate bottle replicates. April 2019 duplicate samples were directly collected from depth by a peristaltic pump fitted with MasterFlex C-flex tubing. All seawater samples were placed in 500 mL borosilicate bottles and fixed with 200 µL saturated mercuric chloride and held at 4 ˚C until laboratory analysis.

A_T was measured with an open-cell titrator using 0.1 M hydrochloric acid titrant on a Metrohm Titrino 848 (Dickson et al., 2007: SOP 3b). Spectrophotometric pH_T measurements were made in duplicate using a Shimadzu 1800 outfitted with a cuvette temperature controller stabilizing temperature at 25 ˚C. The spectrophotometric pH_T was determined using *m*-cresol purple (Acros, batch # 30AXM-QN), following SOP 6b from Dickson et al. (2007). An impurity correction factor of the *m*-cresol reagent was used to adjust the final measured pH_T value (Douglas and Byrne, 2017). All benchtop salinity measurements were conducted with a YSI 3100 conductivity meter. Certified Reference Material of seawater (CRM: Batch 172, A.G., Dickson, Scripps Institute of Oceanography) was used to calculate the A_T and *m*-cresol dye uncertainty. Calibration and reference *in situ* pH_T samples were derived using the Matlab version of CO2SYS (van Heuven et al., 2011) with input parameters salinity, temperature (from thermistor), pH_T, and A_T using carbonic acid dissociation constants from Lueker et al. (2000), the bisulfate dissociation constant of Dickson et al. (1990), and the boron constant from Uppström (1974). Given the broad spectrum of salinity values and low temperatures in this study, potential

uncertainties may be present and difficult to quantify. Dinauer and Mucci (2017) found that dissociation constants derived by Cai and Wang (1998) were best applied to low salinity waters when estimating PCO_2, whereas Lueker constants overestimated values by ≲ 40 µatm. Conversely, Sulpis et al. (2020) found that at low temperatures (< 10 ˚C) Lueker constants underestimated K_1* and K_2* constants resulting in PCO_2 values ~ 20 µatm lower. Given the mostly compensatory nature of salinity and temperature, the Lueker constants provide a medium estimate for the purposes of this study when calibrating across the entire time series.

A SeaFET conditioning period of 9 d was conceded from deployment on 8 August 2018 to 17 August 2018 when the calibration sample was collected. A single-point calibration was applied following previously established best practices (Bresnahan et al., 2014; Miller et al., 2018). New calibration coefficients for the SeaFET were then applied and used to calculate pH_T from the internal ISFET electrode for the entire dataset (Martz et al., 2010). The single reference sample taken on 26 April 2019 was used to compare against SeaFET measured pH_T as a check for sensor drift and robustness of calibration.

2.3.1 Uncertainty estimate

The reliability and accuracy of SeaFET sensors is dependent on estimating the total uncertainty attributable to an individual sensor's behavior and operator usage (Bresnahan et al., 2014; Rivest et al., 2016; McLaughlin et al., 2017; Gonski et al., 2018; Miller et al., 2018). A previous method for calculating the total uncertainty associated with SeaFET function has been previously proposed and was applied to this study (Miller and Kelley *in press*). Briefly, a propagated uncertainty Eq. (1) was derived by adding in quadrate the standard deviation of analytical replicates measuring CRM pH_T spectrophotometrically, a titrator uncertainty comparing

263 measured and known A_T from CRM, the standard deviation of discrete pH_T bottle replicates, and
264 the uncertainty associated with CO2SYS dissociation constants using the Matlab errors function
265 described in Orr et al. (2018). An additional salinity uncertainty not described in Miller and
266 Kelley (*in press*) was added to account for the discrepancy between benchtop salinity
267 measurements and *in situ* readings found in this study (Table S1). The final equation reads:

268 $$Q = \sqrt{\sigma^2_{m-cresol} + \sigma^2_{bottle\ replicates} + \sigma^2_{CO2SYS\ constants} + \sigma^2_{salinity} + AN^2_{titrator}} \quad (1)$$

269 where Q is the propagated uncertainty, AN is the anomaly between measured and known A_T, and
270 σ is the standard deviation of all of the uncertainty input parameters in pH units (see Miller and
271 Kelley 2020 *in press*). From this point, the total uncertainty was calculated by taking the average
272 of the propagated uncertainties for the calibration sample, reference sample, and bottle anomaly
273 (Table 1). This propagated uncertainty was then applied to the entire pH_T time series.
274

275 **2.4 Ancillary data acquisition**

276 The Beaufort Lagoon Ecosystems LTER data on current velocity, water depth, and underwater
277 PAR was accessed through the Environmental Data Initiative portal. Current velocity was used
278 as a proxy to determine the open and closed (i.e., ice-covered or ice-free) seasons for the lagoon.
279 A velocity consistently below 2 cm s^{-1} for a period > 10 h was designated as a threshold for the
280 two phases (Fig. S1). Water depth derived from the pressure sensor was interpreted as tidal
281 variation, where consistent frequencies in depth changes were applied for analysis (see 2.5).
282 Instantaneous PAR measurements were used to determine daily average values for time series
283 analysis.
284

285 **2.5 Frequency Analysis**

A power spectral density (PSD) analysis of pH_T, temperature, salinity, and tide was performed using the *pwelch* function in Matlab (v2020a) to determine the magnitude of variation at a given frequency during each phase: open 2018, closed 2018 – 2019, and open 2019. This function processes data as samples s^{-1}, so for 24 measurements in a day, a sampling rate of 2.78×10^{-4} was applied with a frequency of d^{-1}. A Hamming window was used for sidelobe attenuation (i.e., adjusting width of main peak) of the analyses and the mean value for each parameter was subtracted in order to examine only the variation around the mean. Residual noise around a frequency of zero was muted by applying a Butterworth high-pass filter with an order of three and cut off frequency at 1.0×10^{-5}. If two of the analyzed variables exhibit the same predominant frequency, then their variation is assumed to be correlated regardless of direction and magnitude. Previous PSD analyses with similar parameters have been shown to be considerably noisy below ~ 50 dB Hz^{-1}, thus making this value a cutoff threshold for the purposes of this study (Miller and Kelley *in press*). Frequency peaks corresponding to 1 and 2 d^{-1} are likely a response to the semidiurnal tidal cycle, while a frequency of 3 d^{-1} to daily changes in PAR.

2.6 A_T, PCO_2, and flux calculations

Salinity recorded by the RBR Concerto CTD++ were filtered for invalid measurements taken over the year-long time series. Erroneous data (below the freezing point of water as defined by the temperature-salinity relationship) were removed, and a linear interpolation was performed to replace the missing values (Fig. S2). Two linear regression analyses were performed to estimate A_T, one with measured *in situ* salinity and the other with benchtop recorded values. Each analysis was constructed with the three discrete A_T samples collected on 17 August 2018, 26 April 2019,

and 21 June 2019 (Table S1), where A_T is the dependent variable and salinity the independent. Benchtop values were considered to be more robust as the YSI 3100 Conductivity meter was calibrated to the manufacturer's specification, while the CTD++ was factory calibrated. For this reason, the regression from the benchtop salinity measurements were considered to be the primary hourly A_T values; however, both A_T estimates from benchtop (slope = 59.71, R^2 = 0.968) and *in situ* (slope = 48.38, R^2 = 0.998) salinity were used as input parameters along with measured pH_T to calculate hourly PCO_2 values (Fig. S3) using CO2SYS (see above for constants applied).

Atmospheric hourly PCO_2 averages were collected from the NOAA ESRL station at Barrow (Utqiaġvik), Alaska, USA (Thoning et al., 2020), and wind speed was acquired from automated airport weather observations from the Barter Island Airport. Using these data, a CO_2 air-sea flux for open phases 2018 and 2019 was calculated following the bulk transfer method with a gas transfer velocity constant *k* as modified by the Schmidt number (i.e., ratio of kinematic viscosity of water to gas diffusivity), which is a function of temperature and salinity. The bulk flux equation in Wanninkhof (2014) was used for the estimate:

$$F_{bulk} = 0.251\, U^2\, (Sc/660)^{-0.5}\, K_0\, (PCO_{2_w} - PCO_{2_a}) \qquad (2)$$

where *U* is wind speed in m s^{-1}, *Sc/660* is the Schmidt number calculated using the coefficients from the 4th order polynomial in Wanninkhof (2014: Table 1), K_0 is temperature and salinity dependent solubility of CO_2 in mol L^{-1} atm^{-1} calculated following the model presented in Wanninkhof (2014: Table 2), and PCO_2 is the partial pressure of CO_2 in water ($_w$) and air ($_a$) in atm. The uncertainty applied to the flux estimates are defined as the flux potential given the

broad spectrum of salinity and how it affects the gas transfer velocity and the A_T estimates derived from the *in situ* and benchtop measured salinity values. The flux potential uncertainty was chosen because the values estimated were equal to or more extreme than those identified from the total uncertainty of the pH measurements, if the total pH uncertainty was applied as a proportion to the A_T derived values. Since the Schmidt number is a function of temperature and salinity, a freshwater value was derived using the *fw* coefficients presented in Wanninkhof (2014). This estimate provided a more conservative flux and was, therefore, presented as the lower bound uncertainty in the estimate. The upper bound uncertainty of the flux estimate was calculated by applying the PCO_2 values into Eq. (2) derived from the $salinity_{in\ situ}$-A_T regression. These values resulted in a larger flux estimate, which is why they were set as the upper bound. Both the lower and upper bounds were then applied as the estimated total uncertainty flux potential.

2.7 Statistical methods and data manipulation of pH covariates

Relationships between pH_T and salinity were correlated by applying a 2nd order polynomial fit for the closed 2018 – 2019 phase and open 2019 phase with salinity as the explanatory variable. This included detrending pH_T and reexamining relationships with salinity for open phase 2018 where no correlation was found. Linear regression between temperature and pH_T was performed for each phase of the time series. pH_T and PAR hourly variations were collapsed by calculating the daily averages for both parameters. The average daily values for pH_T open 2018 and 2019 were then detrended to remove correlations with salinity and any potential covariates not captured in this study. A Pearson's correlation coefficient was than derived between the detrended pH_T daily averages and PAR daily averages for open 2018 and open 2019.

355

356 **3 Results**

357 **3.1 Time series**

358 The year-long time series of pH_T, temperature, and salinity was recorded from 17 August 2018 to
359 11 Aug 2019 (Fig. 2). Based on the current velocity threshold of 2 cm s^{-1} as a proxy for sea ice
360 cover, the 2018 open phase transitioned to a closed phase on 8 October 2018 which terminated
361 on 22 June 2019 as the 2019 open phase began (Fig. S1). Both calibration and reference samples
362 that were collected in duplicate have a fairly high standard deviation at 0.099 and 0.088,
363 respectively. The large deviation between duplicate samples was the greatest source of
364 uncertainty (see Eq. 1) for the entire pH_T time series, which shows the total uncertainty shaded in
365 grey (Fig. 2a) and found in (Table 1). Invalid salinity values were ~ 6 % of the entire time series,
366 with the greatest proportion of interpolated values concentrated in the closed phase (Fig.2c).

367 In the open phase of 2018 pH_T values were highly variable in August ranging from 7.66
368 to 8.40, which was the highest pH_T recorded for the entire calendar year (Fig. 3a). An upward
369 trend in pH_T began on 21 August and steadily increased indicating a continued accuracy of the
370 internal ISFET at low salinity. The low episodic salinity event when values were < 9 occurred
371 from 23 August to 27 August 2018, which was after the sporadic variability in pH_T days earlier
372 (Fig. 3). From September until freeze-up on 8 October, pH_T variability was low with the 7-d
373 running average maintaining at ~ 8.10 and fluctuating between 8.07 to 8.18. Temperature
374 followed a steady decrease with a negative slope of 0.12 (Fig. 3b). Salinity rose steadily although
375 instances of large episodic events were present, and in one instance on 1 September, salinity
376 increased from 12.9 to 23.1 in an 8 h period (Fig. 3c).

During the closed phase when Kaktovik Lagoon first became ice-covered, pH_T continued to remain somewhat invariant around ~ 8.10 as it did during the previous two open-water months (Fig. 4a). Approximately 2 weeks into the closed phase, pH_T began to steadily decrease until stabilizing in the beginning of January at ~ 7.71. pH_T varied between 7.55 and 7.85 from this point until April when another negative trend culminated at a low of 7.48. Late May saw pH_T levels increase until phase transition on 22 June 2019. Temperature stayed below -1 ˚C until late May when it began to increase concomitantly with pH_T approaching 0 ˚C (Fig. 4b). Salinity values increased from 31 at the start of ice cover reaching a maximum of 39.2 in April (Fig. 4c).

Open phase 2019 saw extreme pH_T variability beginning 21 June to 11 August 2019 with the rate of hourly change reaching as high as 0.467 units from 7.78 to 8.26 in mid-July (Fig. 5a). During the first portion of this phase, the pH_T running average was consistent at ~ 8.05 with minimal variability. Episodic fluctuations caused pH_T values to reach as high as 8.33. A negative trend began in late July shifting the running average to ~ 7.79, which was lower than the 7.94 running average in August 2018. Temperature increased rapidly during the first 2 weeks following breakup and then remained stable around 10 ˚C (Fig. 5b). Salinity decreased steadily for the first month after breakup followed by large episodic freshening events in late July (Fig. 5c); these were similar to the events seen in the open phase of 2018.

Correlations between salinity and pH_T were inconsistent and varied by phase. Open phase 2018 pH_T was not correlated with salinity which ranged from 5 to 30, while pH_T was predominantly steady shifting only ± 0.1 units around 8.0 (Fig. 6a). A weak negative correlation between temperature and pH_T existed ($R^2 = 0.19$), however removing this trend did not result in changes between salinity and pH_T. The maximum range of pH_T during this period was confined to salinity values between 11.5 to 12.5. During the closed phase, pH_T correlated well with

salinity, which ranged from ~ 30 to 40 (Fig. 6b). An inverse relationship between salinity and pH_T was present during this phase with an R^2 of 0.69. The opposite pattern was observed during open phase 2019, however, where salinity and pH_T were positively correlated with an R^2 of 0.66 (Fig. 6c). Overall, the temperature relationships with salinity were due to seasonal timing rather than intrusion of water mass or mixing. Smoothed data as 7-d running averages between pH_T and temperature, and pH_T and salinity, did not reveal any significant correlations.

3.2 Frequency of pH variability

The PSD of pH_T during open phase 2018 and closed phase 2018 – 2019 were weak with the majority of peaks around any given frequency falling under 50 dB Hz^{-1} (Fig. 7a and b). Peaks of pH_T during open 2018 did not correspond with any regular frequencies across temperature, salinity (Fig. 7) or tide (Fig. S4), which only displayed regular peaks at a frequency of 1 and 2 d^{-1}. Consistent variability of pH_T during the closed phase was negligible but had a maximum magnitude at a frequency of 0.39 which corresponded to a peak observed with temperature (Fig. 7b and e). Open phase 2019 had a multitude of peaks with frequencies ranging from 0.5 to 7.5 d^{-1}, however most fell under 50 dB Hz^{-1} (Fig. 7c). The highest magnitude of pH_T corresponded well with tide at ~ 1 d^{-1} (Fig. 7c and Fig. S4c). Salinity also displayed a strong peak at 1 d^{-1} (Fig. 7i), sharing this frequency of variability with pH_T and tide.

3.3 pH response to PAR

Open phase 2018 and open phase 2019 daily average pH_T was compared against instantaneous underwater PAR levels recorded for both phases (Fig. 8). Open phase 2018 PAR levels were

consistently lower compared to open phase 2019 as a result of the time of year the two phases were observed (Fig. 8). The detrended daily average pH_T correlated well with daily average PAR with a Pearson's correlation coefficient of 0.469 (*p-value* = 0.005). In early August 2018, PAR levels > 5 μmol photons m^{-2} s^{-1} were not representative of, high, daily average pH_T. This was a deviation from the general trend of the open 2018 phase in which daily average pH_T was positively correlated with instantaneous PAR (Fig. 8a). In late August and September, high values of daily average pH_T > 8.20 coincided with spikes in instantaneous PAR that exceeded 10 μmol photons m^{-2} s^{-1} (Fig. 8a).

Open phase 2019 daily average pH_T was overall more variable than open phase 2018 with values from 7.66 in early August to 8.09 in late June (Fig.8b). The detrended daily average pH_T had a more robust correlation with daily average underwater PAR than in 2018 with a Pearson's correlation of 0.643 (*p-value* < 0.001). The highest PAR values were recorded in mid-July; however, this did not correlate with the highest daily average pH_T which was observed in late June. Consistent high values of PAR in mid-July corresponded to relatively flat daily average pH_T (Fig. 8b). A reduction in instantaneous PAR to values below 15 μmol photons m^{-2} s^{-1} in late July was linked with a gradual decrease in daily average pH_T. During this 11-d period, daily average pH_T dropped from 8.06 to 7.71, and only began to increase again when instantaneous PAR exceeded 25 μmol photons m^{-2} s^{-1} for consecutive days.

3.4 Flux Estimation

Carbon flux estimates for open phase 2018 and open phase 2019 showed dramatically different results with 13 instances exceeding a flux > 10 μmol CO_2 m^{-2} min^{-1} compared to 302 instances in open phase 2019 (Fig. 9)—where 10 μmol CO_2 m^{-2} min^{-1} is ≈ to 2 mmol CO_2 m^{-2} d^{-1} which is the

446 equivalent magnitude, but opposite of the estimated annual mean sea-air flux for the coastal
447 Beaufort Sea, -2 mmol CO_2 m^{-2} d^{-1} (Evans et al, 2015a). The episodic events of flux from the
448 atmosphere into seawater was greater in 2018 with 21 instances < -10 μmol CO_2 m^{-2} min^{-1}
449 compared to a single instance in 2019. The maximum lower bound flux potential for open phase
450 2018 was estimated at 2.23 μmol CO_2 m^{-2} min^{-1} whereas the upper bound was 10.67 μmol CO_2
451 m^{-2} min^{-1} (Fig. 9a). Overall, wind speed correlated poorly with CO_2 flux in 2018 (R^2 = 0.13). The
452 highest frequency of robust wind speeds occurred in October but resulted in only a minor
453 atmospheric flux into seawater as the majority of values were between 2 and -5 μmol CO_2 m^{-2}
454 min^{-1} (Fig. 9a).

455 Open phase 2019 had an estimated CO_2 flux as high as 105 μmol CO_2 m^{-2} min^{-1}, which
456 occurred in early August (Fig. 9b). Over a 5.6 d period in late July, CO_2 flux was > 10 μmol CO_2
457 m^{-2} min^{-1} for more than 90 % of the time reaching a high of 78 μmol CO_2 m^{-2} min^{-1}. The
458 maximum lower bound potential flux estimate for open phase 2019 was 5.5 μmol CO_2 m^{-2} min^{-1}
459 with an upper bound of 8.56 μmol CO_2 m^{-2} min^{-1}. Wind speed was found to be significantly
460 correlated with CO_2 flux (*p-value* < 0.0001, R^2 = 0.53) in 2019 and, thus, cogently different from
461 open phase 2018.

462

463 **4 Discussion**

464 Kaktovik Lagoon was an ideal location for a year-long deployment to capture the three phases
465 (i.e., open 2018, closed 2018 – 2019, and open 2019) of environmental conditions in the coastal
466 Arctic. The study site displayed annual pH variability in the context of a unique lagoon where
467 geographical and physical features of this site represent a semi-closed system with narrow
468 passages to the sea and only small tundra stream inputs. The stochastic events of pH captured in

this system are some of the most dramatic hourly pH rates of change recorded to date (Hofmann et al.; 2011; Kapsenberg et al., 2015; Takeshita et al., 2015; Kapsenberg and Hofmann, 2016; Cyronak et al., 2020). These findings represent a system that is often in tenuous equilibrium resulting in dramatic fluctuations of CO_2 outgassing and differing magnitudes of pH sensitivity to temperature and salinity. The extreme nature of these habitats displays the resilience of the micro and macro faunal community that undoubtedly modify seawater pH via biological processes. While this study was able to capture physical and chemical conditions of the lagoon, future work should be directed toward understanding how community organization in the lagoon ecosystem affect pH variability.

4.1 Kaktovik Lagoon and pH-salinity relationship

A crucial finding from this year-long time series was the disparity between the pH_T-salinity relationship during the open 2018, closed 2018 – 2019, and open 2019 phases. Sequentially through the time series, the pH_T-salinity relationship was non-existent, negatively correlated, and positively correlated, indicating that multiple processes drive pH variability at differing magnitudes at a seasonal-phase resolution. Given the myriad processes such as temperature-salinity relationships with carbonate chemistry, current- and wind-driven flux between the sediment-water interface and the air-sea interface, as well as photosynthesis and respiration cycles (Zeebe and Wolf-Gladrow, 2001; Hagens et al., 2014; Carstensen and Duarte, 2019; Rassmann et al., 2020), it is unsurprising that salinity was observed as only a moderate and intermittent driver of pH_T variability in Kaktovik Lagoon. This is despite the multitude of salinity changes that shift in time due to the discharge from rivers and tundra streams, seasonal ice-formation and breakup, and water column stratification, all which would be expected to

fluctuate pH predictably. The features intrinsic to Kaktovik Lagoon are likely important factors responsible for the degree of pH_T-salinity interdependence and provide a lens that elucidates pH_T altering processes that are less germane to physical oceanographic open-ocean mechanisms such as temperature and salinity.

The characteristics of the Beaufort Sea lagoon ecosystems are unique features of the coastline and exist as an interface between terrestrial inputs and seawater with each lagoon varying in its connectivity to the Beaufort and freshwater sources. These lagoons temporarily trap large amounts of allochthonous particulate organic carbon—which is expected to increase with warming temperatures—and sediment as river and stream discharge are temporarily mismatched between spring freshet and ice-covered margins (Dunton et al., 2006; Schreiner et al., 2013). The lagoons adjacent to Kaktovik (Arey and Jago) are likely to be more exogenously influenced due to greater connectivity to the Beaufort Sea, and the Okpilak, Hulahula, and Jago Rivers. Thus, the modification of pH_T within Kaktovik Lagoon provides a baseline that is likely dissimilar to adjacent lagoons providing an in-depth examination of the internal processes of a "closed system" such as biological metabolism and sediment flux that can drive seasonal pH variability and explain the annual shifts in moderate salinity dependence.

In the open phase of 2018, instances of pH_T values and the 7-d running average were observed to be > 8.05 despite the striking range of salinity from 5 to 30. This included an event that modulated salinity from 13 to 23 over an 8 h period, which was correlated with high NW winds at ~ 20 m s^{-1}. This suggests that higher salinity waters from the adjacent Arey Lagoon connecting the Beaufort Sea may have mixed into the bottom waters were the pH sensor was located. The stability of salinity toward the new higher values indicates the validity of this data. Open phase 2019 had a narrower range of salinity which correlated robustly with pH_T as values

above 8.0 were only observed when salinity was > 25. While the interdependence between pH_T and salinity can be variable in nearshore systems (Carstensen and Duarte, 2019), the degree to which pH_T remained stable across a range of salinity in open 2018 is notable. Similarly, a recent study in Stefansson Sound (~ 160 km west of Kaktovik Lagoon) found that salinity-dependent nearshore pH_T varied by year, however, the range of salinity was more attenuated than in Kaktovik (Muth et al. 2020 *in review*). The difference in season between open phase 2018 (fall) and open phase 2019 (summer) could explain some of relational trends between pH_T and salinity. In the fall, storm activity and an abating thermocline can lead to greater vertical mixing, however, the wind data suggest that the incongruity between years was modest. Conversely, the summer breakup is associated with warm temperatures and enhanced freshwater input from ice-melt that can decrease pH. While these factors should be addressed in future studies, the pH trends presented here suggest that in the beginning of August both phases appear to have diverging patterns indicating yearly differences rather than predictable seasonal shifts.

The disparity between the salinity-pH_T correlation between the open 2018 and open 2019 phases was observable in the frequency response of variability. In open phase 2018, the PSD of pH_T was low and mostly incongruent with the frequency response of salinity. This was not the case in open phase 2019 where the highest PSD was recorded at the same frequency (1.03 d^{-1}) as salinity, which was slightly offset from the PSD peak in tidal frequency at 0.98 d^{-1}. These associations suggest that events driving low salinity such as stream runoff were likely too irregular, or too low of flux, relative to the weak but consistent tidal signal driving open ocean exchange. This also corresponds to the lower range of salinity observed in open phase 2019 than in open phase 2018.

4.2 High-frequency pH in Arctic and Subarctic

Interannual variability of pH_T between open phase 2018 and open phase 2019 is not dependent on a single driving factor, including time of season. In the 2018 open phase pH_T was consistently high during a period when daylength was shortening and temperatures were falling. The increasing trend of consistently high pH_T continued into the closed phase. Conversely, August 2019 pH_T had a running average that was ~ 0.2 units lower than 2018 and continued a downward trend until the end of the time series. Similar findings have shown significantly different interannual variability in pH along the Arctic coast that exceeded the running average difference of ~ 0.2 observed in Kaktovik Lagoon by double (Muth et al. *in review)*. This seasonally shifting dependence of pH_T on salinity has implications for carbonate chemistry dynamics and how pH_T is modified. Freshwater input from rivers have been shown to increase dissolved inorganic carbon and lower A_T which can decouple the linear relationships between calcium carbonate saturation state, PCO_2, and pH (Salisbury et al., 2008; Cai, 2011; Hales et al., 2016). Glacial ice-melt in subarctic waters, however, is unique in that its profile is low in PCO_2 and A_T (Evans et al., 2014). Both modes of freshwater carbonate chemistry decoupling may be present in Kaktovik, but evidence here suggests that salinity is a non-reliable indicator of these decoupling mechanisms as pH_T values can exist across a wide range of salinity and even lack relationship during open phases.

Open phase 2019 displayed highly variable pH_T relative to open phase 2018 with an inconsistent frequency of variability. In the subarctic waters off Alaska's south-central coast, Jakolof Bay had a consistent seasonal trend in pH_T variability with hourly rates of change as high as 0.18 from ~ 7.801 to 7.981 (Miller and Kelley 2020, *in press*). While these rates of hourly change are considered high (Hofmann et al., 2011), both open phases in Kaktovik were more

than double that (0.401 and 0.467 from 7.655 – 8.056 and 7.789 – 8.255, respectively) of Jakolof Bay. These extreme rates of change in Kaktovik can be partially explained by the photosynthetic and respiratory activity within the lagoon.

4.3 PAR and pH

This study found robust correlations between underwater PAR and daily average pH_T. The episodic nature of pH_T variability in Kaktovik Lagoon was more prevalent during periods of high underwater PAR indicative of coupled diurnal photosynthesis-respiration cycles. Consistent levels of PAR appeared to be associated with sustained daily average pH_T while drops in PAR lowered the overall baseline pH_T. The rapid response of baseline pH_T to PAR highlights the tenuous balance between the biological processes that drive pH_T modification. This phenomenon is counter to what was observed in the subarctic macroalgal-dominated waters of Jakolof Bay where the system maintained net autotrophy for a period > 60 days (Miller and Kelley, *in press*). Possible explanations for the precarity of a dominant autotrophic or heterotrophic system may be due to the shallow nature of the lagoon and frequent homogeneity of the water column. In the shallow waters of the lagoon, high winds easily resuspend organic material, enhance respiration, and increase light attenuation (Capuzzo et al., 2015; Moriarty et al., 2018). Thus, small decreases in underwater PAR can lead to net heterotrophy. This supports the sediment "food bank" hypothesis as continuous primary production is not needed to sustain heterotrophic activity, since stored, labile, benthic OM can accumulate in shallow environments fueling respiration (Mincks et al., 2005; Harris et al., 2018). A "bank" of OM could explain why high levels of PAR led to a sustained pH_T, and any instantaneous drop in PAR was immediately followed a decrease in daily average pH_T. This would suggest that high levels of PAR are only able to offset high rates of

584 heterotrophy which are sustained by the seasonal accumulation of carbon subsidies from
585 autochthonous ice algae, phytoplankton, and influx of OM from terrestrial sources—which are
586 likely to vary annual.
587
588 **4.4 Sea ice effects on carbonate chemistry**
589 A unique feature of ice-covered Arctic coastal waters is the negative relationship between pH_T
590 and salinity, which was observed here and in previous studies (Nomura et al., 2006; Miller et al.,
591 2011; Fransson et al., 2013; Muth et al., *in review*). In the open ocean, salinity is positively
592 correlated with A_T as higher salinity increases the difference between conservative cations to
593 anions. Furthermore, A_T positively correlates with pH, and a higher A_T is associated with a
594 higher buffering capacity. The formation of sea ice, however, induces cryoconcentration of DIC
595 and A_T via active rejection of HCO_3^- during freezing and exclusion of other ions, lowering pH
596 and creating high salinity brine drainage (Miller et al., 2011; Fransson et al., 2013; Hare et al.,
597 2013). The immediate effect of high DIC concentration can lead to the precipitation of $CaCO_3$ in
598 the form of ikaite (a polymorph of $CaCO_3 \cdot 6H_2O$) along the bottom of bulk ice formation
599 generating CO_2 as a product of the reaction and leading to greater decreases in pH (Rysgaard et
600 al., 2012; Fransson et al., 2013; Hare et al., 2013). In addition, the extreme salinity and
601 temperature in winter affect carbonate chemistry by modulating solubility, where an increase in
602 salinity decreases CO_2 solubility, and colder temperatures increase CO_2 solubility. These salinity
603 and temperature conditions result in a volatile thermodynamic stability of CO_2 where salinity
604 effects outweigh temperature effects and can facilitate a degassing of CO_2 (Papadimitriou et al.,
605 2004).

606 The continually decreasing pH_T observed in this study suggests that these carbon
607 concentrating corollaries of sea ice formation may be in effect and contribute to the negative
608 relationship observed between pH_T and salinity. That is, if there is no outgassing of CO_2, the
609 relative increase in DIC and concomitant decrease in pH will be equal to that of salinity. During
610 ice coverage, the running average of pH_T decreased from 7.93 in the beginning of November, to
611 7.56 in late April, and mirrors the under-ice salinity trend. This decrease is nearly identical to the
612 0.4 pH drop (~ 8.15 to 7.75) observed in the upper 2 m below the ice in Amundsen Gulf from the
613 November to April period (Fransson et al., 2013). While this phenomenon could partially explain
614 the general decreasing trend between pH_T and salinity, it would be remiss to state that this
615 negative correlation is entirely driven by cryoconcentration and ikaite formation. Assuming the
616 A_T-salinity regression calculated here is similar to a DIC-salinity correlation from
617 cryoconcentration, the decrease in pH_T would not be great enough to explain the observations in
618 the lagoon. While ikaite formation may be present, and further decreasing pH, the driving factor
619 to bring the A_T:DIC ratio below 1 [which would be needed to see pH ~ 7.55] is likely the
620 accumulation of respired CO_2 occurring tangentially with salinity decrease. Following a general
621 stoichiometric relationship between N and C to be 16:106, and assuming trivial efflux of N from
622 the sediment, the change in surface NH_4^+ from August 2018 to April 2019 would be equal to a
623 130 µmol kg^{-1} increase in DIC over this period (Table S1) sufficiently decreasing the A_T:DIC
624 ratio below 1. We note that the PO_4^{3-} values are a bit anomalous, but these concentrations depend
625 on the N:P ratio in the remineralized OM and flux of solutes from the sediment.
626
627 **4.5 Under ice variability in pH**

628 The frequency of pH_T variability under ice cover was inconsistent. The PSD was weak overall
629 during the closed phase but had a peak at 0.39 d^{-1}, which corresponded to a peak in temperature
630 around the same frequency 0.36 d^{-1}. The temperature range of 1.9 ˚C during the closed phase can
631 affect carbonate chemistry thermodynamics potential modulating pH by ~ 0.036; however, this is
632 less than the derived pH_T uncertainty. The other factor driving pH_T variability is biological
633 respiration. Data sonde measurements of dissolved oxygen recorded in late April showed bottom
634 waters reaching lows of 156.3 µmol L^{-1} (43 % saturation) compared to surface levels of 359.5
635 µmol L^{-1} (94 % saturation) (Table S1). The stratification of oxygen in this case can likely be
636 associated with burgeoning PAR levels in April. Previous studies have shown increases in pH
637 are associated with photosynthesis during ice-cover, which is more prevalent proximal to bulk
638 ice resulting in higher pH at the surface compared to the bottom (Matson et al., 2014). Other
639 factors driving pH variability could be due to the competition between anaerobic and aerobic
640 metabolism in low oxygenated water, and the transfer of reduced metabolites from bioirrigation
641 (Aller, 1982, 2001; Zakem et al., 2020). Efflux of reduced metabolites from the sediment can
642 lead to high concentrations of reduced inorganic nitrogen if oxygen concentrations are low and
643 oxidation processes slow (Aller, 2001; Middelburg and Levin, 2009). Discrete samples taken in
644 April found high concentrations of reduced nitrogen in the bottom waters (Table S1). If oxygen
645 levels begin to increase in late spring due to photosynthesis, the subsequent oxidation of nitrogen
646 and other accumulated reduced metabolites could decrease pH as was seen from mid-April to
647 mid-May. Due to limited under-ice sampling, however, there is no way to determine the
648 trajectory of oxygen decrease or exact timing of under ice photosynthesis. The only other
649 mechanism potentially supplying oxygen to the lagoon would be associated with water mass
650 exchange via tide. According to the frequency analysis, there is limited evidence showing a

651 correlated frequency peak between pH_T and tide, indicating that tidal exchange may be restricted
652 or not a modulator of pH_T during the closed phase. Without measuring dissolved oxygen,
653 however, it remains unclear if oxygen is the determinant factor driving pH_T modification during
654 the closed phase.
655
656 **4.6 Arctic lagoons as carbon source to atmosphere**
657 The estimates of CO_2 flux during the open phases of 2018 and 2019 were an *a posteriori* method
658 to examine the drivers of pH variability in Kaktovik Lagoon. Following this approach,
659 comparisons between pH_T rate of change and estimated CO_2 flux did not correlate, suggesting
660 that outgassing rates were not significant enough to raise *in situ* pH. Rather, the analysis showed
661 that the estimated lagoon CO_2 flux varied substantially by year and appears at times to be a
662 source of CO_2 to the atmosphere. This is counter to other studies that measured carbon flux at a
663 lagoon in the far western Beaufort (Elson Lagoon), where this site was categorized as a carbon
664 sink; however, these lagoons differ in size, residence time, and connectivity to adjacent water
665 bodies (Lougheed et al., 2020). Overall, the western Arctic Ocean is thought to be a carbon sink (
666 Laruelle et al., 2014; Evans et al., 2015a); although Mathis et al. (2012) described occasional
667 storm-induced upwelling events across the Beaufort Sea shelf that cause CO_2 efflux to the
668 atmosphere. In this study, the variability in estimated flux from the lagoon appeared to be a
669 function of baseline pH_T more than wind-driven stress. Open phase 2018 had a higher baseline
670 pH_T (8.01 – 8.18) than open phase 2019 (8.04 – 7.72), and despite wind speeds comparable to
671 open phase 2019, resulted in a lower estimated CO_2 efflux to the atmosphere. Conversely, open
672 phase 2019 maintained a lower baseline pH_T which promoted favorable disequilibrium (i.e.,
673 difference between PCO_{2sw} and PCO_{2a}) conditions that only needed wind stress as a catalyst.

Since flux preceded low pH_T values, and outgassing did not decrease hourly pH_T, the mechanisms driving low pH and PCO_2—likely biological respiration— transcend the counterbalance of outgassing. Similar conclusions were found in a boreal lake where wind-driven stress reduced the thermocline and induced CO_2 upwelling that counterbalanced CO_2 loss from surface waters to the atmosphere (Åberg et al., 2010). In relation to this study, it would be logical to conclude that the reason wind speed was correlated to open phase 2019 and not open phase 2018 flux was due to a lower baseline pH and PCO_2 at the surface as a result of enhanced CO_2 upwelling from benthic respiration in the early portion of the open phase. Since open phase 2018 measurements were taken in the latter portion of the season, benthic fluxes of CO_2 may have been exhausted as terrestrial OM abundance diminished with time.

The flux estimates in this study suggest that the novel characteristics of coastal lagoons should be considered anomalous compared to the greater across shelf Arctic coast, defined as waters north of 70 ˚N and west of 100 ˚W (Bakker et al., 2014). The current classification of the coastal Arctic does not account for lagoons as specific ecosystems. Thus, the western Arctic coastal ocean is defined as a relatively homogenous area 1.2×10^{12} m^2 along the Chukchi and Beaufort Seas extending 400 km offshore (Evans et al., 2015a). The coastal Beaufort Sea under this definition is estimated to have an annual mean carbon uptake of 8.5 Tg C yr^{-1} without ice, and a daily annual mean flux of -2.1 mmol CO_2 m^{-2} d^{-1} (Evans et al., 2015a). Recent evidence, however, has shown that previous estimates of the carbon sink capacity of the Arctic Ocean have been overestimated, suggesting that current and increasing riverine discharge will cause a reduction in A_T ultimately decreasing its potential to absorb CO_2 (Woosley and Millero, 2020). While the lagoon ecosystems comprise a small proportion of the greater Beaufort Sea shelf, they encompass > 50 % of its coastline with significant freshwater inputs that can lower the carbon

sink capacity (Dunton et al., 2006; Woosley and Millero, 2020). It is suggested here that certain lagoons, including Kaktovik, are likely episodic sources of CO_2 to the atmosphere during open phases. The net daily average (± s.d.) CO_2 flux for Kaktovik Lagoon during open phase 2018 and 2019 was -2.2 ± 6.5 and 14.6 ± 23.9 mmol CO_2 m^{-2} d^{-1}, respectively. Over the entire calendar year that encompasses both open phases during which sensors were deployed, the annual daily average flux was 5.9 ± 19.3 mmol CO_2 m^{-2} d^{-1} for the entire calendar year. If integrated over the entire open phase (51.58 d in 2018 and 49.38 d in 2019), and the area of Kaktovik Lagoon, estimates suggest a net carbon flux of -2.68 x 10^{-5} Tg C $open_{18}^{-1}$ in open 2018 and 1.67 x 10^{-4} Tg C $open_{19}^{-1}$ in open 2019. Over an entire calendar year this equates to 1.40 x 10^{-4} Tg C yr^{-1}.

It is noted that these estimates are for incomplete open phases as the data presented here do not comprise the entirety of each seasons due the scheduling of SeaFET deployment and recovery. If incorporating all the lagoons along the coast, it is plausible that the source of CO_2 from the lagoon ecosystems would partially offset the carbon sink capacity previously established, particularly when considering that the estimated daily annual average flux is at times substantially greater (5.9 ± 19.3 mmol CO_2 m^{-2} d^{-1}), and opposite, of current estimates (-2.1 mmol CO_2 m^{-2} d^{-1}) (Evans et al., 2015a; Mathis et al., 2015). Further studies that can capture high-frequency carbonate chemistry variability are needed though to determine the degree and frequency of the Beaufort lagoon ecosystems' air-sea carbon exchange.

There is a fair amount of confidence in these estimates because the A_T-salinity correlation was robust (R^2 = 0.968) and the regression coefficients were proximal to other A_T-salinity regressions for the Gulf of Alaska and the western coastal Arctic, despite being derived from only three discrete samples (Yamamoto-Kawai et al., 2005; Shadwick et al., 2011; Evans et al., 2015b). Processes such as terrestrial runoff of organic alkalinity and ice-melt can increase

uncertainties in the A_T-salinity relationship; however, ice-melt induced deviations appeared negligible in the Gulf of Alaska (Cai et al., 1998; Evans et al., 2014). Further, the overall uncertainty calculated as a flux potential was low. The main source of deviation was associated with higher PCO_2 values calculated from the A_T-salinity$_{in\ situ}$ regression. This made up the upper bound, thus, the conclusions drawn here are from the more conservative flux estimates. The effect of fresh water on the gas transfer velocity comprised the lower bound and was negligible overall. For the flux estimates presented here, a homogenous water column with respect to pH was assumed, given that discrete sonde measurements only showed pH stratification during the closed phase (Table S1). This is not to suggest that salinity and temperature driven stratification do not exist, rather that the evidence here suggests pH_T water column homogeneity. For example, pH_T during open phase 2018 did not correlate with salinity as values > 8.01 were present across a salinity range of 25. In cases where pH_T positively correlated with salinity as seen during open phase 2019, a freshwater stratification would suggest that low salinity at the surface would be associated with lower pH_T, and likely increase the CO_2 flux as there would be a greater disequilibrium between the lagoon and the air. According to the quadratic fit between pH_T and salinity, lower pH_T at the surface associated with freshwater stratification would outweigh the A_T estimates based on salinity by an order of magnitude if there was a salinity difference of 10 between the surface and bottom waters. Thus, freshwater stratification at the surface would likely exceed our upper bound potential flux estimate and increase efflux rates. Further, any modulation of flux by temperature on the gas transfer velocity are less than the estimated upper bound and considered negligible.

5 Conclusions

743 This study presents the first high-frequency pH time series for the open and under ice phases in
744 the coastal Arctic lagoon system. Uncertainty estimates for pH_T were higher than desired but
745 describe general trends and relative rates of change that are informative for understanding pH
746 variability. The extremely low anomaly between the reference pH_T sample and the SeaFET
747 suggest that the uncertainty is likely lower than estimated. pH can vary dramatically by year for
748 the open phases and is likely a function of PAR availability and the amount of OM delivered
749 from terrestrial sources as the balance between system autotrophy and heterotrophy were
750 tenuous. This resulted in hourly pH_T rates of change > 0.4 units (~ 7.7 – 8.1). Under ice pH
751 variability exhibited complexities, and we postulate that multiple drivers of pH variability such
752 as carbonate chemistry thermodynamics, accumulation of respired CO_2, ikaite precipitation, and
753 sediment efflux were all contributing mechanisms. It is apparent that further studies of carbonate
754 chemistry dynamics at the sediment-water interface are needed to help elucidate porewater
755 effects on bottom water pH variability during the closed, ice-covered phase, as well as
756 continuous oxygen measurements. Estimated CO_2 outgassing during the open phase was not a
757 significant factor driving pH_T variability due to the collinearity of wind stress and the infrequent
758 convergence between disequilibrium and wind speed. However, carbon flux estimates suggest
759 that the Beaufort lagoon ecosystems may be a substantial source of carbon to the atmosphere,
760 which is counter to previous studies predicting coastal Arctic waters as a CO_2 sink. This may
761 have further implications meaning that periods of CO_2 efflux from the lagoon system may
762 increase as the extent of ice-fee days increases in the coming decades with warmer temperatures.
763 These results highlight the need for further investigation of the Beaufort lagoon ecosystems in
764 the context of carbonate chemistry dynamics, as these processes can affect the diverse biological

communities that are present here, and aid in understanding western coastal Arctic biogeochemical dynamics.

Data availability: All data accessed from the Beaufort Lagoon Ecosystems LTER is available on the Environmental Data initiative:

Beaufort Lagoon Ecosystems LTER and J. Kasper. 2020. Circulation dynamics: currents, waves, temperature measurements from moorings in lagoon sites along the Alaska Beaufort Sea coast, 2018-ongoing ver 2. Environmental Data Initiative. https://doi.org/10.6073/pasta/3475cdbb160a9f844aa5ede627c5f6fe

Beaufort Lagoon Ecosystems LTER, Core Program. 2020. Photosynthetically active radiation (PAR) time series from lagoon sites along the Alaska Beaufort Sea coast, 2018-ongoing ver 1. Environmental Data Initiative. https://doi.org/10.6073/pasta/ced2cedd430d430d9149b9d7f1919729

Beaufort Lagoon Ecosystems LTER, Core Program. 2020. physicochemical water column parameters and hydrographic time series from river, lagoon, and open ocean sites along the Alaska Beaufort Sea coast, 2018-ongoing ver 1. Environmental Data Initiative. https://doi.org/10.6073/pasta/e0e71c2d59bf7b08928061f546be6a9a

Beaufort Lagoon Ecosystems LTER, Core Program. 2020. Time series of water column pH from lagoon sites along the Alaska Beaufort Sea coast, 2018-ongoing ver 1. Environmental Data Initiative. https://doi.org/10.6073/pasta/9305328d0f1ed28fbb2d7cf56c686786

Author Contributions: Cale A. Miller, NM, CB, and ALK conceptualized the manuscript thesis. CAM performed all data analysis and data visualization. ALK performed initial data QA/QC for pH data. ALK, NM, and CB performed lab analyses. CAM wrote the original manuscript draft with minor contributions in the introduction from ALK and CB in the methods. ALK, CB, and NM reviewed and edited the manuscript.

Competing interests: The authors declare no conflict of interest.

Acknowledgments: We thank R/V Proteus captains Ted Dunton and John Dunton for expert mooring deployment and recovery. We additionally thank K. Dunton, S. Jump, J. Kasper for logistical and field assistance. This work took place in the traditional and current homeland of the Kaktovikmuit.

Financial support: This material is based upon work supported by the National Science Foundation under award #1656026

References

Åberg, J., Jansson, M. and Jonsson, A.: Importance of water temperature and thermal stratification dynamics for temporal variation of surface water CO_2 in a boreal lake, J. Geophys. Res. Biogeosciences, 115(G2), doi:https://doi.org/10.1029/2009JG001085, 2010.

Aller, R.: Carbonate Dissolution in Nearshore Terrigenous Muds - the Role of Physical and Biological Reworking, J. Geol., 90(1), 79–95, 1982.

Aller, R.C.: Transport and reactions in the bioirrigated zone, in: The Benthic Boundary Layer: Transport Processes and Biogeochemistry, edited by: Boudreau, B. P. and Jorgensen, B. B., pp. 269–301, Oxford University Press., 2001.

Bakker, D. C. E., Pfeil, B., Smith, K., Hankin, S., Olsen, A., Alin, S. R., Cosca, C., Harasawa, S., Kozyr, A., Nojiri, Y., O'Brien, K. M., Schuster, U., Telszewski, M., Tilbrook, B., Wada, C., Akl, J., Barbero, L., Bates, N. R., Boutin, J., Bozec, Y., Cai, W.-J., Castle, R. D., Chavez, F. P., Chen, L., Chierici, M., Currie, K., de Baar, H. J. W., Evans, W., Feely, R. A., Fransson, A., Gao, Z., Hales, B., Hardman-Mountford, N. J., Hoppema, M., Huang, W.-J., Hunt, C. W., Huss, B., Ichikawa, T., Johannessen, T., Jones, E. M., Jones, S. D., Jutterström, S., Kitidis, V., Körtzinger, A., Landschützer, P., Lauvset, S. K., Lefèvre, N., Manke, A. B., Mathis, J. T., Merlivat, L., Metzl, N., Murata, A., Newberger, T., Omar, A. M., Ono, T., Park, G.-H., Paterson, K., Pierrot, D., Ríos, A. F., Sabine, C. L., Saito, S., Salisbury, J., Sarma, V. V. S. S., Schlitzer, R., Sieger, R., Skjelvan, I., Steinhoff, T., Sullivan, K. F., Sun, H., Sutton, A. J., Suzuki, T., Sweeney, C., Takahashi, T., Tjiputra, J., Tsurushima, N., van Heuven, S. M. a. C., Vandemark, D., Vlahos, P.,

826 Wallace, D. W. R., Wanninkhof, R. and Watson, A. J.: An update to the Surface Ocean CO_2
827 Atlas (SOCAT version 2), Earth Syst. Sci. Data, 6(1), 69–90, doi:https://doi.org/10.5194/essd-6-
828 69-2014, 2014.

829 Beaufort Lagoon Ecosystems LTER and J. Kasper. 2020. Circulation dynamics: currents, waves,
830 temperature measurements from moorings in lagoon sites along the Alaska Beaufort Sea coast,
831 2018-ongoing ver 2. Environmental Data Initiative.
832 https://doi.org/10.6073/pasta/3475cdbb160a9f844aa5ede627c5f6fe
833
834 Beaufort Lagoon Ecosystems LTER, Core Program. 2020. Photosynthetically active radiation
835 (PAR) time series from lagoon sites along the Alaska Beaufort Sea coast, 2018-ongoing ver 1.
836 Environmental Data Initiative.
837 https://doi.org/10.6073/pasta/ced2cedd430d430d9149b9d7f1919729
838
839 Beaufort Lagoon Ecosystems LTER, Core Program. 2020. physicochemical water column
840 parameters and hydrographic time series from river, lagoon, and open ocean sites along the
841 Alaska Beaufort Sea coast, 2018-ongoing ver 1. Environmental Data Initiative.
842 https://doi.org/10.6073/pasta/e0e71c2d59bf7b08928061f546be6a9a
843
844 Beaufort Lagoon Ecosystems LTER, Core Program. 2020. Time series of water column pH from
845 lagoon sites along the Alaska Beaufort Sea coast, 2018-ongoing ver 1. Environmental Data
846 Initiative. https://doi.org/10.6073/pasta/9305328d0f1ed28fbb2d7cf56c686786
847
848 Bresnahan, P. J., Martz, T. R., Takeshita, Y., Johnson, K. S. and LaShomb, M.: Best practices for
849 autonomous measurement of seawater pH with the Honeywell Durafet, Methods Oceanogr., 9,
850 44–60, doi:10.1016/j.mio.2014.08.003, 2014.

851 Cai, W.-J., Wang, Y. and Hodson, R. E.: Acid-Base Properties of Dissolved Organic Matter in
852 the Estuarine Waters of Georgia, USA, Geochim. et Cosmochim. Acta, 62(3), 473–483,
853 doi:10.1016/S0016-7037(97)00363-3, 1998.
854
855 Cai, W.-J. and Wang, Y.: The chemistry, fluxes, and sources of carbon dioxide in the estuarine
856 waters of the Satilla and Altamaha Rivers, Georgia, Limnology and Oceanography, 43(4), 657–
857 668, doi:https://doi.org/10.4319/lo.1998.43.4.0657, 1998.

858 Cai, W.-J.: Estuarine and Coastal Ocean Carbon Paradox: CO_2 Sinks or Sites of Terrestrial
859 Carbon Incineration?, in Annual Review of Marine Science, Vol 3, vol. 3, edited by C. A.
860 Carlson and S. J. Giovannoni, pp. 123–145, Annual Reviews, Palo Alto., 2011.

861 Capuzzo, E., Stephens, D., Silva, T., Barry, J. and Forster, R. M.: Decrease in water clarity of the
862 southern and central North Sea during the 20th century, Glob. Change Biol., 21(6), 2206–2214,
863 doi:10.1111/gcb.12854, 2015.

864 Carstensen, J. and Duarte, C. M.: Drivers of pH Variability in Coastal Ecosystems, Environ. Sci.
865 Technol., 53(8), 4020–4029, doi:10.1021/acs.est.8b03655, 2019.

Craig, P. C.: Subsistence fisheries at coastal villages in the Alaskan Arctic, 1970–1986. Biological Papers of the University of Alaska, 24, 131-152, 1989.

Cyronak, T., Takeshita, Y., Courtney, T. A., DeCarlo, E. H., Eyre, B. D., Kline, D. I., Martz, T., Page, H., Price, N. N., Smith, J., Stoltenberg, L., Tresguerres, M. and Andersson, A. J.: Diel temperature and pH variability scale with depth across diverse coral reef habitats, Limnol. Oceanogr. Lett., 5(2), 193–203, doi:10.1002/lol2.10129, 2020.

Dickson, A.: Thermodynamics of the Dissociation of Boric-Acid in Potassium-Chloride Solutions from 273.15-K to 318.15-K, J. Chem. Eng. Data, 35(3), 253–257, doi:10.1021/je00061a009, 1990.

Dickson A. G., Sabine C. L. & Christian J. R.: Guide to best practices for ocean CO_2 measurements, in: PICES Special Publication, edited by: Dickson, A. G., Sabine, C. L., and Christian, J. R., 2007.

Dinauer, A. and Mucci, A.: Spatial variability in surface-water pCO_2 and gas exchange in the world's largest semi-enclosed estuarine system: St. Lawrence Estuary (Canada), Biogeosciences, 14(13), 3221–3237, doi:https://doi.org/10.5194/bg-14-3221-2017, 2017.

Douglas, N. K. and Byrne, R. H.: Achieving accurate spectrophotometric pH measurements using unpurified meta-cresol purple, Mar. Chem., 190, 66–72, doi:10.1016/j.marchem.2017.02.004, 2017.

Dunton, K.H., and S.V. Schonberg.: Barter Island to Demarcation Bay: A preliminary benthic survey of Arctic coastal lagoons. Fairbanks: Final Report to USF&WS, Arctic Refuge, 2006.

Dunton, K. H., Weingartner, T. and Carmack, E. C.: The nearshore western Beaufort Sea ecosystem: Circulation and importance of terrestrial carbon in arctic coastal food webs, Prog. Oceanogr., 71(2), 362–378, doi:10.1016/j.pocean.2006.09.011, 2006.

Dunton, K. H., Schonberg, S. V. and Cooper, L. W.: Food Web Structure of the Alaskan Nearshore Shelf and Estuarine Lagoons of the Beaufort Sea, Estuaries Coasts, 35(2), 416–435, doi:10.1007/s12237-012-9475-1, 2012.

Evans, W., Mathis, J. T. and Cross, J. N.: Calcium carbonate corrosivity in an Alaskan inland sea, Biogeosciences, 11(2), 365–379, doi:10.5194/bg-11-365-2014, 2014.

Evans, W., Mathis, J. T., Cross, J. N., Bates, N. R., Frey, K. E., Else, B. G. T., Papkyriakou, T. N., DeGrandpre, M. D., Islam, F., Cai, W.-J., Chen, B., Yamamoto-Kawai, M., Carmack, E., Williams, W. J. and Takahashi, T.: Sea-air CO_2 exchange in the western Arctic coastal ocean, Glob. Biogeochem. Cy., 29(8), 1190–1209, doi:10.1002/2015GB005153, 2015a.

Evans W., Mathis, J. T., Ramsey, J. and Hetrick J.: On the frontline: Tracking ocean acidification in an Alaskan shellfish hatchery, PloS One, 10(7), e0130384, doi:10.1371/journal.pone.0130384, 2015b.

907 Fabry, V., McClintock, J., Mathis, J. and Grebmeier, J.: Ocean Acidification at High Latitudes:
908 The Bellwether, Oceanogr., 22(4), 160–171, doi:10.5670/oceanog.2009.105, 2009.

909 Fransson, A., Chierici, M., Miller, L. A., Carnat, G., Shadwick, E., Thomas, H., Pineault, S. and
910 Papakyriakou, T. N.: Impact of sea-ice processes on the carbonate system and ocean acidification
911 at the ice-water interface of the Amundsen Gulf, Arctic Ocean, J. Geophys. Res. Oceans,
912 118(12), 7001–7023, doi:10.1002/2013JC009164, 2013.

913 Gonski, S. F., Cai, W.-J., Ullman, W. J., Joesoef, A., Main, C. R., Pettay, D. T. and Martz, T. R.:
914 Assessment of the suitability of Durafet-based sensors for pH measurement in dynamic estuarine
915 environments, Estuar. Coast. Shelf Sci., 200, 152–168, doi:10.1016/j.ecss.2017.10.020, 2018.

916 Griffiths, W.B., J.K. Den Beste, and P.C.: Fisheries investigations in a coastal lagoon region of
917 the Beaufort Sea (Kaktovik Lagoon, Alaska). Arctic Gas Biol. Report Ser. 40(2): 1–190, 1977.
918
919 Hagens, M., Hunter, K. A., Liss, P. S. and Middelburg, J. J.: Biogeochemical context impacts
920 seawater pH changes resulting from atmospheric sulfur and nitrogen deposition, Geophys. Res.
921 Lett., 41(3), 935–941, doi:10.1002/2013GL058796, 2014.

922 Hales, B., Suhrbier, A., Waldbusser, G. G., Feely, R. A. and Newton, J. A.: The Carbonate
923 Chemistry of the "Fattening Line," Willapa Bay, 2011–2014, Estuar. Coast., 1–14,
924 doi:10.1007/s12237-016-0136-7, 2016.

925 Hare, A. A., Wang, F., Barber, D., Geilfus, N.-X., Galley, R. J. and Rysgaard, S.: pH evolution
926 in sea ice grown at an outdoor experimental facility, Mar. Chem., 154, 46–54,
927 doi:10.1016/j.marchem.2013.04.007, 2013.

928 Harris, C. M., McClelland, J. W., Connelly, T. L., Crump, B. C. and Dunton, K. H.: Salinity and
929 Temperature Regimes in Eastern Alaskan Beaufort Sea Lagoons in Relation to Source Water
930 Contributions, Estuar. Coast., 40(1), 50–62, doi:10.1007/s12237-016-0123-z, 2017.

931 Harris, C. M., McTigue, N. D., McClelland, J. W. and Dunton, K. H.: Do high Arctic coastal
932 food webs rely on a terrestrial carbon subsidy?, Food Webs, 15, e00081,
933 doi:10.1016/j.fooweb.2018.e00081, 2018.

934 Hofmann, G. E., Smith, J. E., Johnson, K. S., Send, U., Levin, L. A., Micheli, F., Paytan, A.,
935 Price, N. N., Peterson, B., Takeshita, Y., Matson, P. G., Crook, E. D., Kroeker, K. J., Gambi, M.
936 C., Rivest, E. B., Frieder, C. A., Yu, P. C. and Martz, T. R.: High-Frequency Dynamics of Ocean
937 pH: A Multi-Ecosystem Comparison, Plos One, 6(12), e28983,
938 doi:10.1371/journal.pone.0028983, 2011.

939 Johnson, S. W., Thedinga, J. F., Neff, A. D., & Hoffman, C. A.: Fish fauna in nearshore waters
940 of a barrier island in the western Beaufort Sea, Alaska, 2010.
941
942 Kapsenberg, L. and Hofmann, G. E.: Ocean pH time-series and drivers of variability along the
943 northern Channel Islands, California, USA, Limnol. Oceanogr., 61(3), 953–968,
944 doi:10.2307/26628461, 2016.
945

946 Kapsenberg, L., Kelley, A. L., Shaw, E. C., Martz, T. R. and Hofmann, G. E.: Near-shore
947 Antarctic pH variability has implications for the design of ocean acidification experiments, Sci.
948 Rep., 5, srep09638, doi:10.1038/srep09638, 2015.
949
950 Kinney, P., Schell, D., Dygas, J., Nenahlo, R. and Hall, G.: Nearshore Currents, in: Baseline data
951 study of the Alaskan Arctic aquatic environment, Kinney, P., Schell, D., Alexander, V., Burrell,
952 D., Cooney, R. and Naidu, A. S., Univ. Alaska, Inst. Mar. Sci. Rep. R-72-3, 1971.
953
954 Kraus, N. C., Patsch, K. and Munger, S.: Barrier Beach Breaching from the Lagoon Side, With
955 Reference to Northern California, U.S. Army Engineer Research and Development Center, Coast
956 and Hydraulics Laboratory, 2008.
957
958 Laruelle, G. G., Lauerwald, R., Pfeil, B. and Regnier, P.: Regionalized global budget of the CO_2
959 exchange at the air-water interface in continental shelf seas, Glob. Biogeochem. Cy., 28(11),
960 1199–1214, doi:10.1002/2014GB004832, 2014.

961 Lissauer, I. M., Hachmeister, L. E., Morson, B. J.: Atlas of the Beaufort Sea, U.S. Dep. of Trans.,
962 U.S. Coast Guard, Office of Res. and Dev., 1984.

963 Lougheed, V. L., Tweedie, C. E., Andresen, C. G., Armendariz, A.M., Escarzaga, S. M. and
964 Tarin, G.: Patterns and drivers of carbon dioxide concentration sin aquatic ecosystems of the
965 Arctic coastal tundra, Glob. Biogeochem. Cy., 34(3), e2020GB006552,
966 doi:10.1029/2020GB006552, 2020.
967
968 Lueker, T. J., Dickson, A. G. and Keeling, C. D.: Ocean pCO_2 calculated from dissolved
969 inorganic carbon, alkalinity, and equations for K_1 and K_2: Validation based on laboratory
970 measurements of CO_2 in gas and seawater at equilibrium, Mar. Chem., 70(1), 105–119,
971 doi:10.1016/S0304-4203(00)00022-0, 2000.

972 Macdonald, R.W., E. Sakshaug, and R. Stein.: The Arctic Ocean: modern status and recent
973 climate change, in: The organic carbon cycle in the Arctic Ocean, edited by: R. Stein and R.W.
974 Macdonald, pp. 6–21, Berlin: Springer, 2004.
975

976 Martz, T. R., Connery, J. G. and Johnson, K. S.: Testing the Honeywell Durafet® for seawater
977 pH applications, Limnol. Oceanogr. Methods, 8(5), 172–184, doi:10.4319/lom.2010.8.172, 2010.

978 Mathis, J. T., Pickart, R. S., Byrne, R. H., McNeil, C. L., Moore, G. W. K., Juranek, L. W., Liu,
979 X., Ma, J., Easley, R. A., Elliot, M. M., Cross, J. N., Reisdorph, S. C., Bahr, F., Morison, J.,
980 Lichendorf, T. and Feely, R. A.: Storm-induced upwelling of high pCO_2 waters onto the
981 continental shelf of the western Arctic Ocean and implications for carbonate mineral saturation
982 states, Geophys. Res. Lett., 39(7), L07606, doi:10.1029/2012GL051574, 2012.

983 Mathis, J. T., Cross, J. N., Evans, W. and Doney, S. C.: Ocean Acidification in the Surface
984 Waters of the Pacific-Arctic Boundary Regions, Oceanogr., 28(2), 122–135,
985 doi:10.5670/oceanog.2015.36, 2015.

Matson, P. G., Washburn, L., Martz, T. R. and Hofmann, G. E.: Abiotic versus Biotic Drivers of Ocean pH Variation under Fast Sea Ice in McMurdo Sound, Antarctica, PloS One, 9(9), e107239, doi:10.1371/journal.pone.0107239, 2014.

Matthews, J. B. and Stringer, W. J.: Spring breakup and flushing of an Arctic lagoon estuary, J. Geophys. Res. Oceans, 89(C2), 2073–2079, doi:10.1029/JC089iC02p02073, 1984.

McClelland, J. W., Déry, S. J., Peterson, B. J., Holmes, R. M. and Wood, E. F.: A pan-arctic evaluation of changes in river discharge during the latter half of the 20th century, Geophys. Res. Lett., 33(6), doi:10.1029/2006GL025753, 2006.

McClelland, J. W., Holmes, R. M., Dunton, K. H. and Macdonald, R. W.: The Arctic Ocean Estuary, Estuar. Coast., 35(2), 353–368, doi:10.1007/s12237-010-9357-3, 2012.

McClelland, J. W., Townsend-Small, A., Holmes, R. M., Pan, F., Stieglitz, M., Khosh, M. and Peterson, B. J.: River export of nutrients and organic matter from the North Slope of Alaska to the Beaufort Sea, Water Resor. Res., 50(2), 1823–1839, doi:10.1002/2013WR014722, 2014.

McLaughlin, K., Dickson, A., Weisberg, S. B., Coale, K., Elrod, V., Hunter, C., Johnson, K. S., Kram, S., Kudela, R., Martz, T., Negrey, K., Passow, U., Shaughnessy, F., Smith, J. E., Tadesse, D., Washburn, L. and Weis, K. R.: An evaluation of ISFET sensors for coastal pH monitoring applications, Reg. Stud. Mar. Sci., 12, 11–18, doi:10.1016/j.rsma.2017.02.008, 2017.

Middelburg, J. J. and Levin, L. A.: Coastal hypoxia and sediment biogeochemistry, Biogeosciences, 6(7), 1273–1293, doi:https://doi.org/10.5194/bg-6-1273-2009, 2009.

Miller, C. A., Pocock, K., Evans, W. and Kelley, A. L.: An evaluation of the performance of Sea-Bird Scientific's SeaFET™ autonomous pH sensor: considerations for the broader oceanographic community, Ocean Sci., 14(4), 751–768, doi:https://doi.org/10.5194/os-14-751-2018, 2018.

Miller, C. A. and Kelley A. K.: Seasonality and biological forcing the diel frequency of nearshore pH extremes in a sub-arctic Alaskan estuary, Limnol. Oceanogr., *in press*, doi: 10.1002/lno.11698, 2021.

Miller, L. A., Carnat, G., Else, B. G. T., Sutherland, N. and Papakyriakou, T. N.: Carbonate system evolution at the Arctic Ocean surface during autumn freeze-up, J. Geophys. Res. Oceans, 116(C9), doi:10.1029/2011JC007143, 2011.

Miller, L. A., Macdonald, R. W., McLaughlin, F., Mucci, A., Yamamoto-Kawai, M., Giesbrecht, K. E. and Williams, W. J.: Changes in the marine carbonate system of the western Arctic: patterns in a rescued data set, Polar Res., 33(1), 20577, doi:10.3402/polar.v33.20577, 2014.

Mincks, S. L., Smith, C. R. and DeMaster, D. J.: Persistence of labile organic matter and microbial biomass in Antarctic shelf sediments: evidence of a sediment 'food bank,' Marine Ecol. Prog. Ser., 300, 3–19, 2005.

Moriarty, J. M., Harris, C. K., Friedrichs, M. A. M., Fennel, K. and Xu, K.: Impact of Seabed Resuspension on Oxygen and Nitrogen Dynamics in the Northern Gulf of Mexico: A Numerical Modeling Study, J. Geophys. Res. Oceans, 123(10), 7237–7263, doi:10.1029/2018JC013950, 2018.

Mouillot, D., Dumay, O. and Tomasini, J. A.: Limiting similarity, niche filtering and functional diversity in coastal lagoon fish communities, Estuar. Coast. Shelf Sci., 71(3), 443–456, doi:10.1016/j.ecss.2006.08.022, 2007.

Muth, A., Kelley, A. K. and Dunton, K.: High-Frequency pH Time-Series Reveals Pronounced Seasonality in Arctic Coastal Waters, Limnol. Oceanogr., *in review*.

Nomura, D., Yoshikawa-Inoue, H. and Toyota, T.: The effect of sea-ice growth on air–sea CO_2 flux in a tank experiment, Tellus B Chem. Phys. Meteorol., 58(5), 418–426, doi:10.1111/j.1600-0889.2006.00204.x, 2006.

Orr, J. C., Epitalon, J.-M., Dickson, A. G. and Gattuso, J.-P.: Routine uncertainty propagation for the marine carbon dioxide system, Mar. Chem., 207, 84–107, doi:10.1016/j.marchem.2018.10.006, 2018.

Papadimitriou, S., Kennedy, H., Kattner, G., Dieckmann, G. S. and Thomas, D. N.: Experimental evidence for carbonate precipitation and CO_2 degassing during sea ice formation, Geochim. Cosmochim. Acta, 68(8), 1749–1761, doi:10.1016/j.gca.2003.07.004, 2004.

Qi, D., Chen, L., Chen, B., Gao, Z., Zhong, W., Feely, R. A., Anderson, L. G., Sun, H., Chen, J., Chen, M., Zhan, L., Zhang, Y. and Cai, W.-J.: Increase in acidifying water in the western Arctic Ocean, Nat. Clim. Change, 7(3), 195–199, doi:10.1038/nclimate3228, 2017.

Rassmann, J., Eitel, E. M., Lansard, B., Cathalot, C., Brandily, C., Taillefert, M. and Rabouille, C.: Benthic alkalinity and dissolved inorganic carbon fluxes in the Rhône River prodelta generated by decoupled aerobic and anaerobic processes, Biogeosciences, 17(1), 13–33, doi:https://doi.org/10.5194/bg-17-13-2020, 2020.

Rivest, E. B., O'Brien, M., Kapsenberg, L., Gotschalk, C. C., Blanchette, C. A., Hoshijima, U. and Hofmann, G. E.: Beyond the benchtop and the benthos: Dataset management planning and design for time series of ocean carbonate chemistry associated with Durafet®-based pH sensors, Ecol. Inform., Complete(36), 209–220, doi:10.1016/j.ecoinf.2016.08.005, 2016.

Robards, M. D.: Coastal lagoon community and ecological monitoring in the Southern Chukchi Sea National Park Unit over five decades- Status and 2012 field sampling report. National Park Service, Fairbanks, AK, 2014.

Rysgaard, S., Glud, R. N., Lennert, K., Cooper, M., Halden, N., Leakey, R. J. G., Hawthorne, F.C. and Barber, D.: Ikaite crystals in melting sea ice - implications for pCO_2 and pH levels in Arctic surface waters, The Cryos., 6, 901–908, doi:10.5194/tc-6-901-2012, 2012.

Salisbury, J. E., Vandemark, D., Hunt, C. W., Campbell, J. W., McGillis, W. R. and McDowell, W. H.: Seasonal observations of surface waters in two Gulf of Maine estuary-plume systems:

Relationships between watershed attributes, optical measurements and surface pCO_2, Estuar. Coast. Shelf Sci., 77(2), 245–252, doi:10.1016/j.ecss.2007.09.033, 2008.

Schreiner, K. M., Bianchi, T. S., Eglinton, T. I., Allison, M. A. and Hanna, A. J. M.: Sources of terrigenous inputs to surface sediments of the Colville River Delta and Simpson's Lagoon, Beaufort Sea, Alaska, J. Geophys. Res. Biogeosciences, 118(2), 808–824, doi:10.1002/jgrg.20065, 2013.

Shadwick, E. H., Thomas, H., Chierici, M., Else, B., Fransson, A., Michael, C., Miller, L. A., Mucci, A., Niemi, A., Papakyriakou, T. N. and Tremblay, J.-E.: Seasonal variability of the inorganic carbon system in the Amundsen Gulf region of the southeastern Beaufort Sea, Limnol. Oceanogr., 56(1), 303–322, doi:10.4319/lo.2011.56.1.0303, 2011.

Stein, R. and Macdonald, R. W.: Organic carbon budget: Arctic Ocean vs. Global Ocean in: The organic carbon cycle in the Arctic Ocean, edited by: R. Stein and R.W. Macdonald, pp. 315–322, Berlin: Springer, 2004.

Sulpis, O., Lauvset, S. K. and Hagens, M.: Current estimates of K_1* and K_2* appear inconsistent with measured CO_2 system parameters in cold oceanic regions, Ocean Science, 16(4), 847–862, doi:https://doi.org/10.5194/os-16-847-2020, 2020.

Takeshita, Y., Frieder, C. A., Martz, T. R., Ballard, J. R., Feely, R. A., Kram, S., Nam, S., Navarro, M. O., Price, N. N. and Smith, J. E.: Including high-frequency variability in coastal ocean acidification projections, Biogeosciences, 12(19), 5853–5870, doi:https://doi.org/10.5194/bg-12-5853-2015, 2015.

Thoning, K. W., Crotwell, A. M. and J. W. Mund.: Atmospheric Carbon Dioxide Dry Air Mole Fractions from continuous measurements at Mauna Loa, Hawaii, Barrow, Alaska, American Samoa, and South Pole. 1973-2019, Version 2020-08 Notional Oceanic and Atmospheric Administration (NOAA), Global Monitoring Laboratory (GML), Boulder, Colorado, USA http://doi.org/10.151138/yaf1-bk21 FTP pat: ftp://aftp.cmdl.noaa.gov/data/greenhouse_gases/co2/in-situ/surface/

Tibbles, M.: The seasonal dynamics of coastal Arctic lagoons in Northwest Alaska, M.Sc. thesis, December. College of Fisheries and Ocean Sciences, University of Alaska Fairbanks, 2018.

Uppström, L. R.: The boron/chlorinity ratio of deep-sea water from the Pacific Ocean, Deep Sea Res. Oceanogr. Abstr., 21, 161–162, doi:10.1016/0011-7471(74)90074-6, 1974.

van Heuven, S., Pierrot, D., Rae, J. W. B., Lewis, E., and Wallace, D.W. R.: MATLAB Program Developed for CO_2 System Calculations Department of Energy, Oak Ridge, Tennessee, 2011.

Wanninkhof, R.: Relationship between wind speed and gas exchange over the ocean revisited, Limnol. Oceanogr. Methods, 12(6), 351–362, doi:10.4319/lom.2014.12.351, 2014.

Woosley, R. J. and Millero, F. J.: Freshening of the western Arctic negates anthropogenic carbon uptake potential, Limnol. Oceanogr., 65(8), 1834–1846, doi:10.1002/lno.11421, 2020.

Wynn, J. G., Robbins, L. L. and Anderson, L. G.: Processes of multibathyal aragonite undersaturation in the Arctic Ocean, J. Geophys. Res. Oceans, 121(11), 8248–8267, doi:10.1002/2016JC011696, 2016.

Yamamoto-Kawai, M., Tanaka, N. and Pivovarov, S.: Freshwater and brine behaviors in the Arctic Ocean deduced from historical data of δO^{18} and alkalinity (1922–2022 A.D.), J. Geophys. Res. Oceans, 110(C10), doi:10.1029/2004JC002793, 2005.

Zakem, E. J., Mahadevan, A., Lauderdale, J. M. and Follows, M. J.: Stable aerobic and anaerobic coexistence in anoxic marine zones, ISME J., 14(1), 288–301, doi:10.1038/s41396-019-0523-8, 2020.

Zeebe, R. E. and Wolf-Gladrow, D. A.: CO_2 in seawater equilibrium, kinetics, isotopes, Elsevier, Amsterdam; New York., 2001.

Zhang, Y., Yamamoto-Kawai, M. and Williams, W. J.: Two Decades of Ocean Acidification in the Surface Waters of the Beaufort Gyre, Arctic Ocean: Effects of Sea Ice Melt and Retreat From 1997–2016, Geophys. Res. Lett., 47(3), e60119, doi:10.1029/2019GL086421, 2020.

Table 1. Calibration and reference bottle data for SeaFET. Propagated uncertainty, for each bottle, and the calculated total pH uncertainty value as overall average (in bold). Value marked with * indicates the calibration bottle sample.

Date & Time	*Source*	*pH_T internal electrode*	*Propagated uncertainty*	*Anomaly: | bottle sample - SeaFET |*
17 Aug. 2018	SeaFET	8.076	—	
	Bottle sample	8.073*	0.1600	—
26 Apr. 2018	SeaFET	7.576	—	
	Bottle sample	7.582	0.1006	0.0061
Total uncertainty				**0.0889**

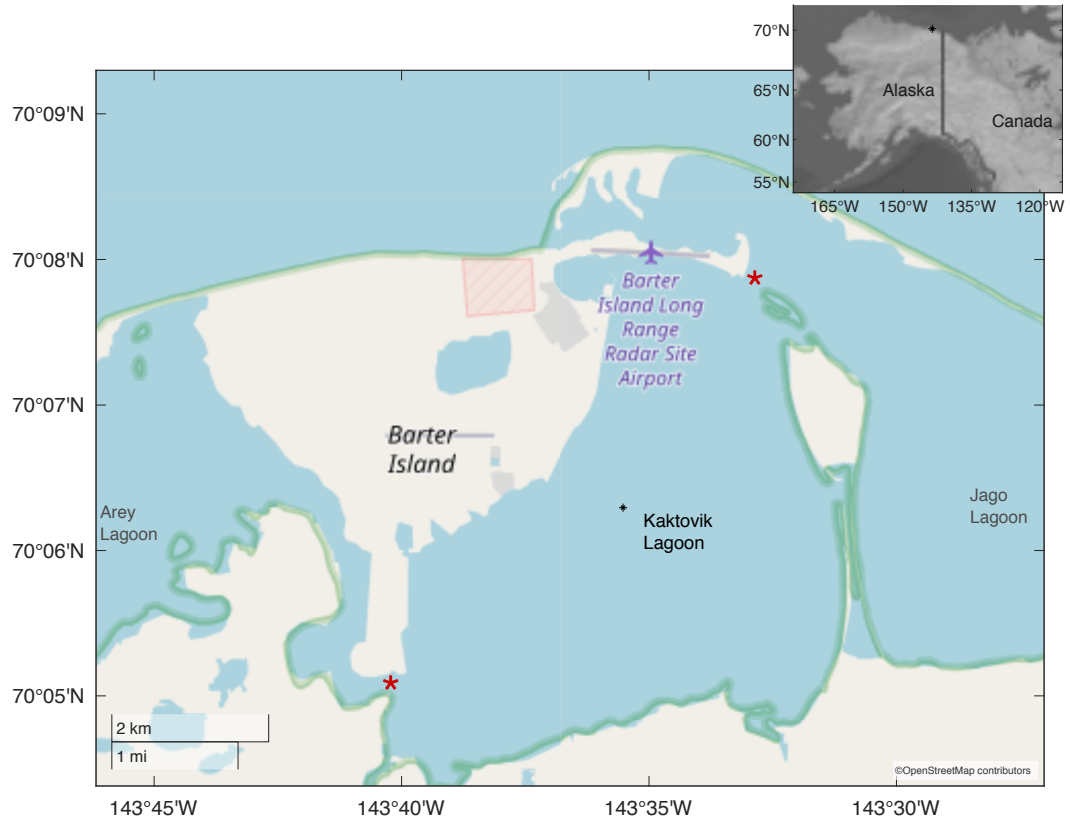

Figure 1. Study site at Kaktovik Lagoon along the Beaufort Sea Coastline. Red stars denote the main exchange pathways between adjacent lagoons and greater Beaufort Sea. Black star in inset map is location of Kaktovik Lagoon.

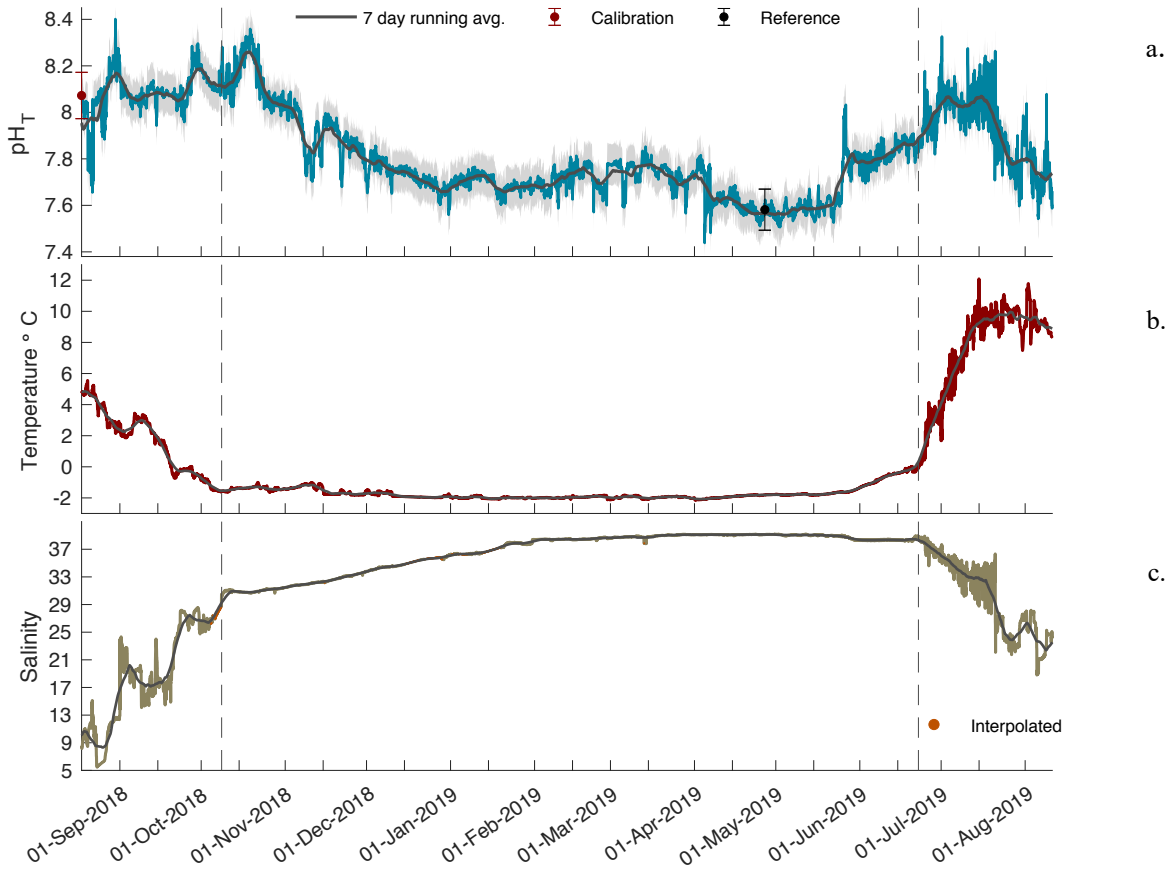

Figure 2. Times series of pH_T (a), temperature (b), and salinity (c) in Kaktovik Lagoon for entire deployment period from 17 August 2018 to 11 August 2019. The first section to the left of the dashed line is open phase 2018, the middle section is closed 2018 – 2019, and the last section to the right of the second dashed line is open phase 2019.

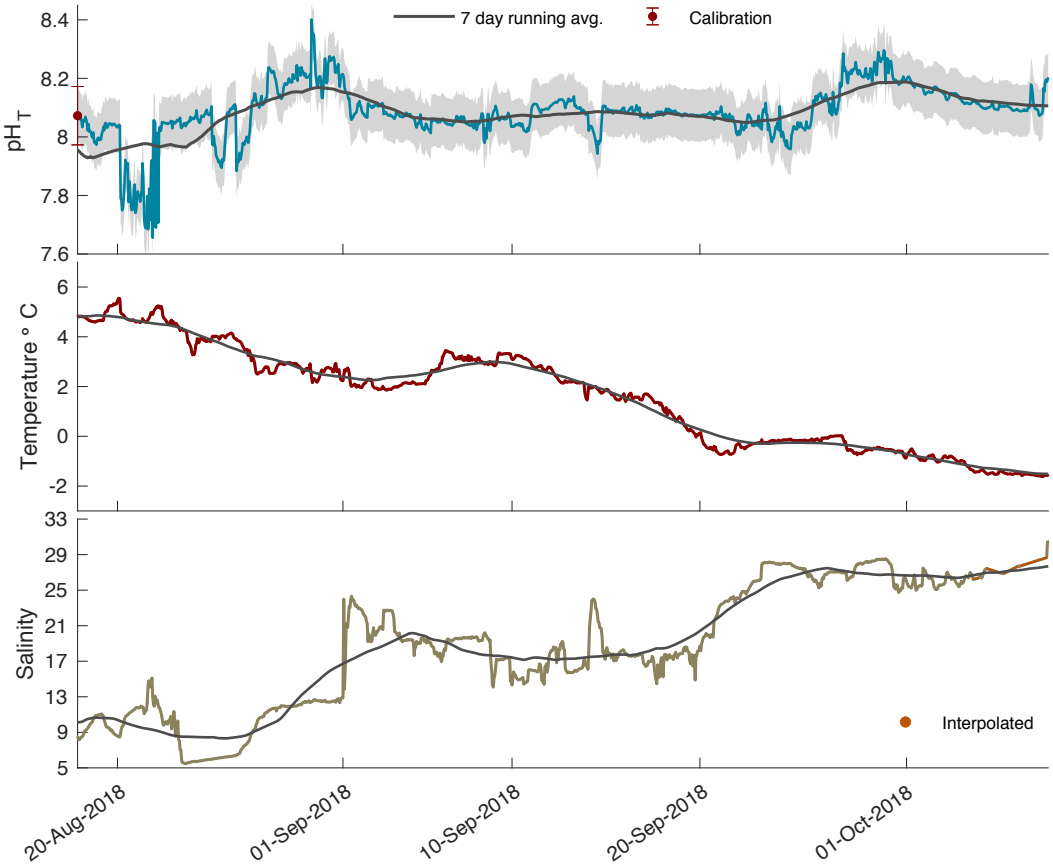

Figure 3. Open phase 2018 time series of pH_T (a), temperature (b), and salinity (c) in Kaktovik Lagoon.

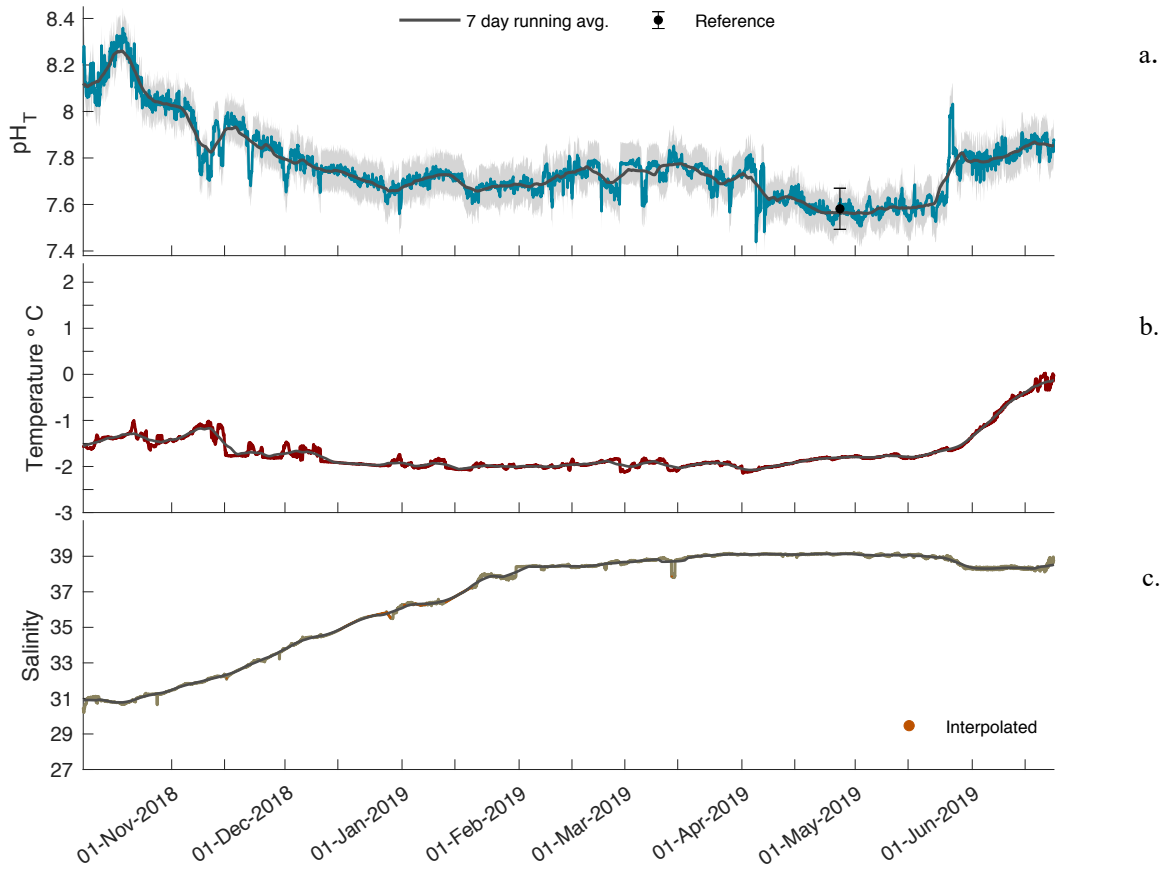

Figure 4. Closed phase 2018 – 2019 time series of pH_T (a), temperature (b), and salinity (c) in Kaktovik Lagoon.

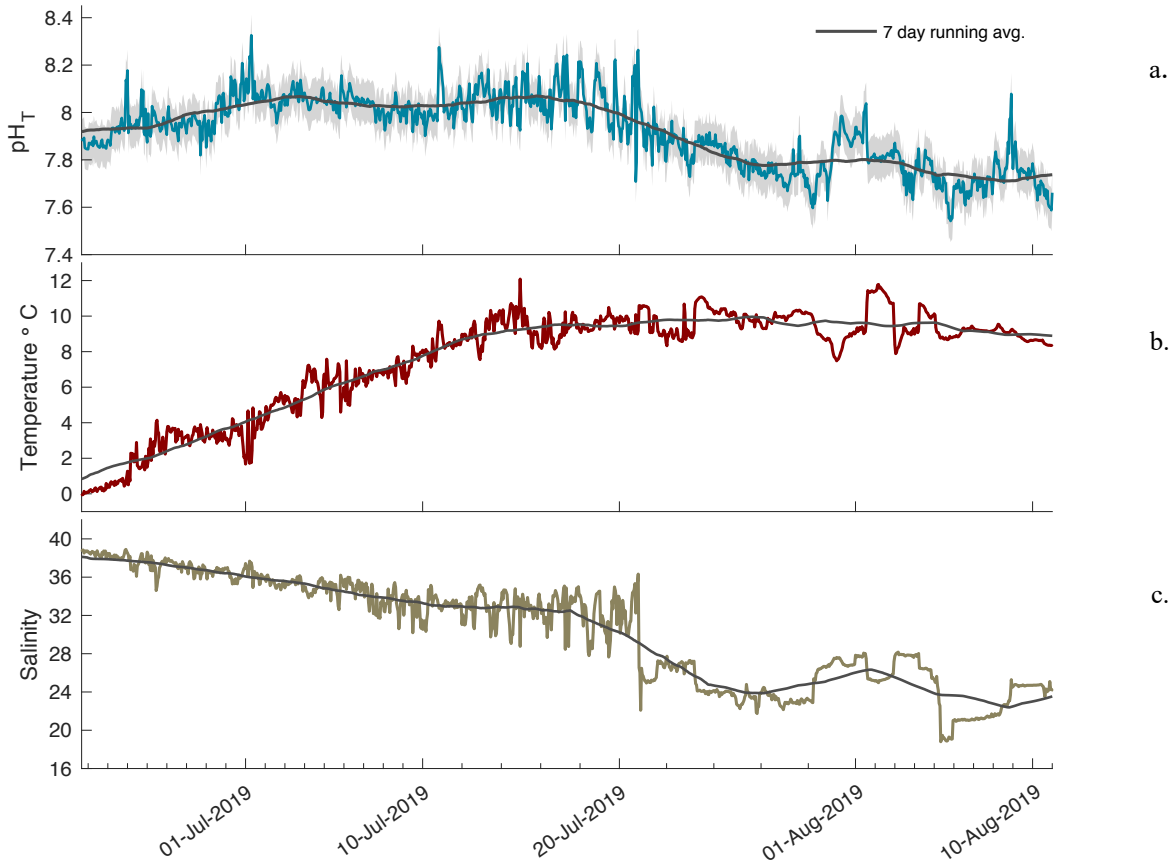

Figure 5. Open phase 2019 time series of pH_T (a), temperature (b), and salinity (c) in Kaktovik Lagoon.

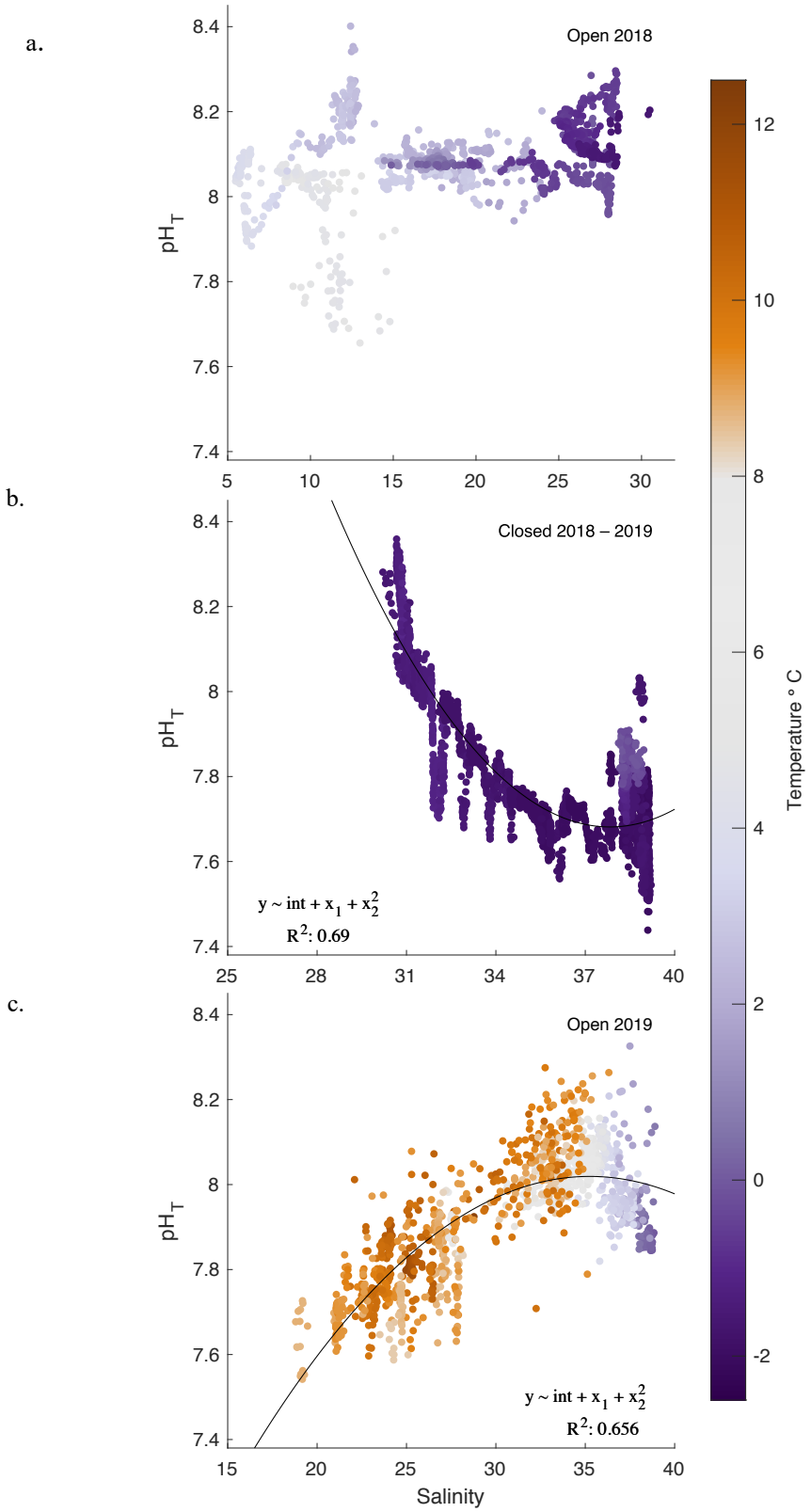

Figure 6. pH_T-salinity correlations for open 2018 (**a**), Closed 2018 – 2019 (**b**), and open 2019 (**c**). Quadratic fits are applied to iced and open 2019 phases only. Temperature is represented in color for all correlations.

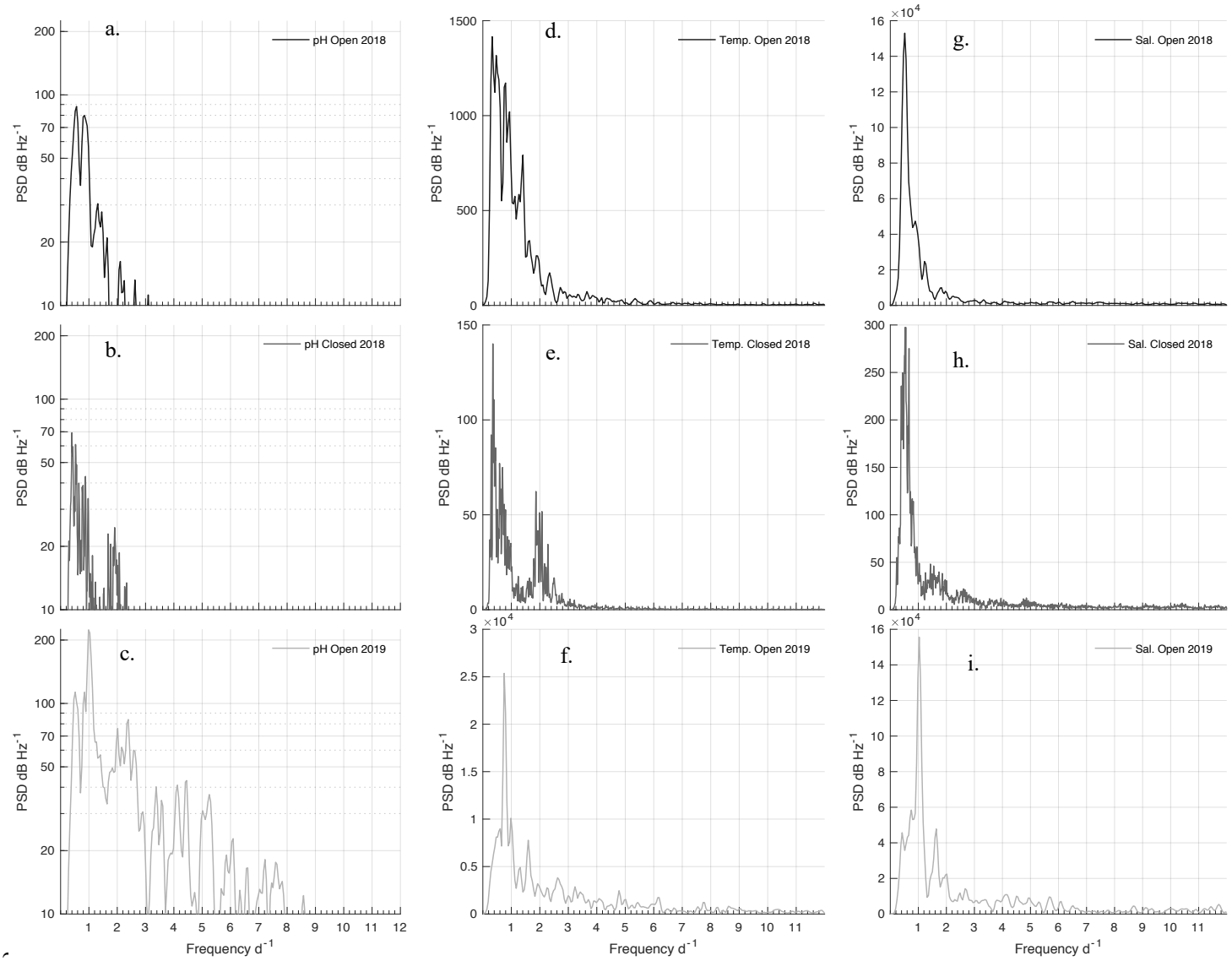

Figure 7. Power Spectral Density (PSD) plots for pH_T (a,b,c), temperature (d,e,f), and salinity (g,h,i) at each phase of the time series: open 2018 (top row), Closed 2018 – 2019 (middle row), and open 2019 (bottom row).

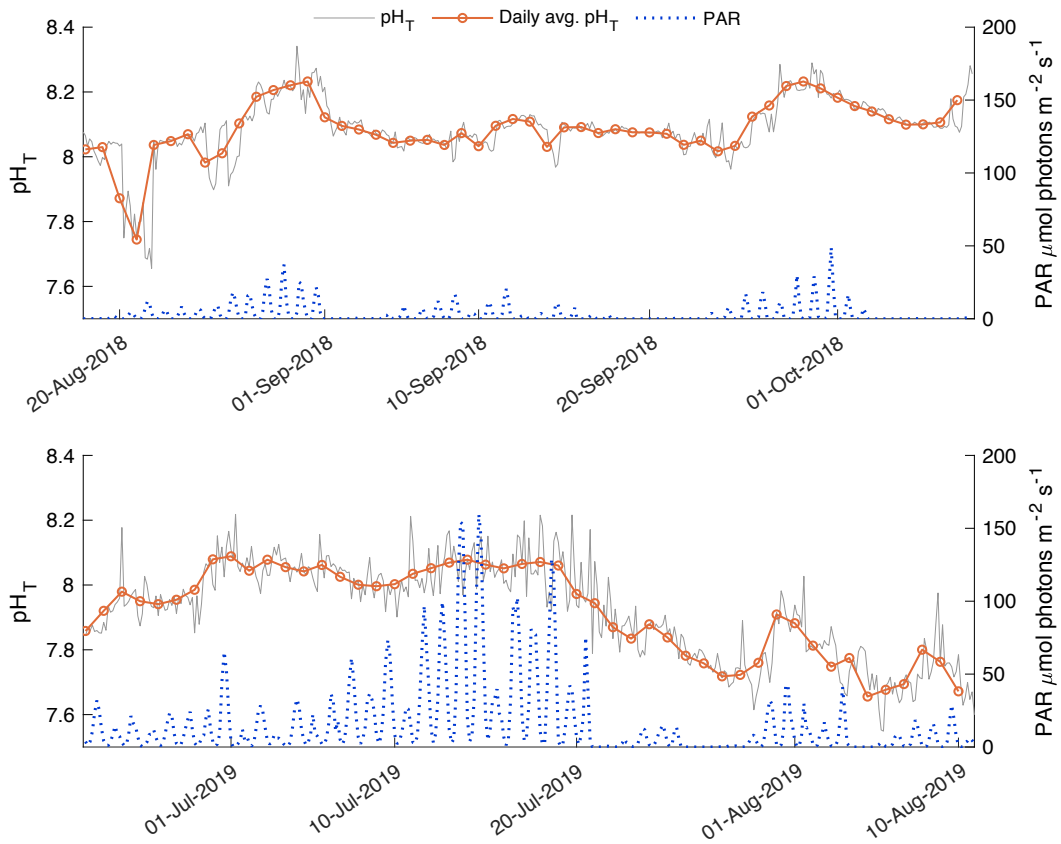

Figure 8. Detrended pH_T (gray line) and PAR (blue dots) for open phase 2018 (**a**) and open phase 2019 (**b**). Daily average pH_T (orange line) is displayed overtop hourly variability.

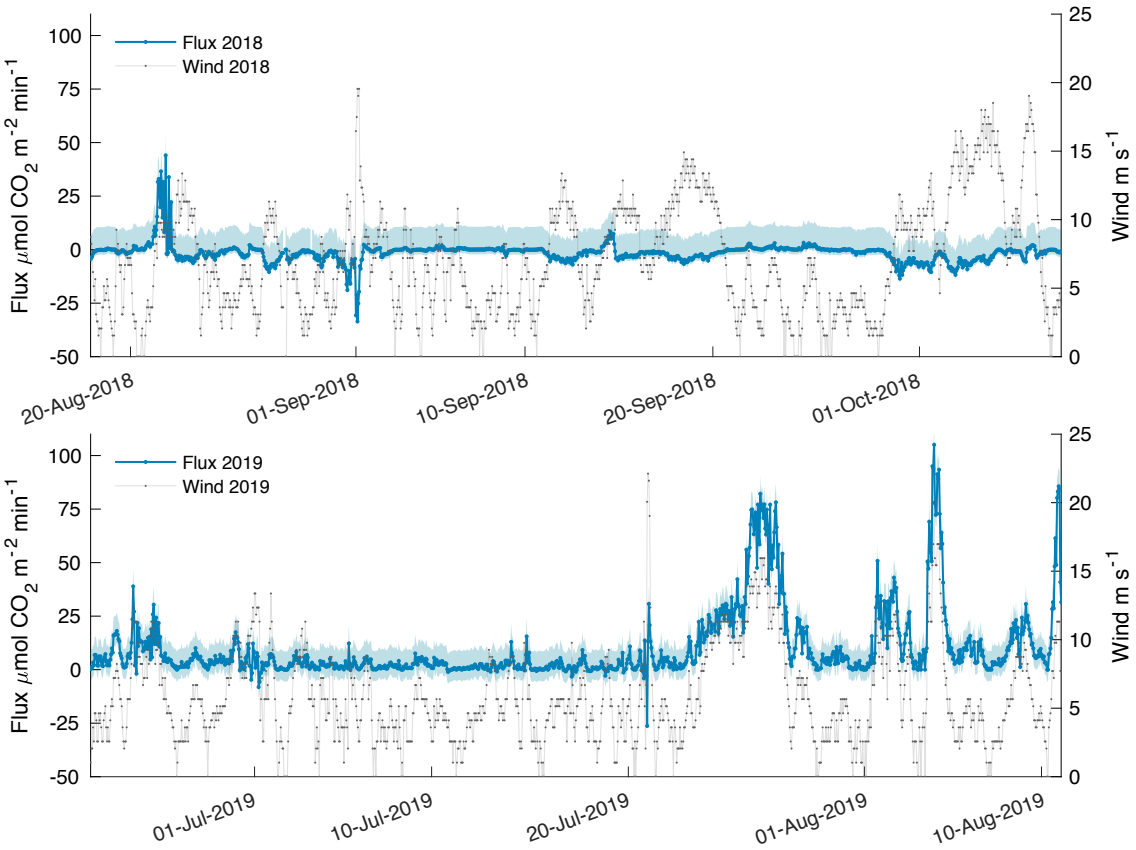

Figure 9. Estimated carbon flux (orange) and wind speed (grey) for open phase 2018 (**a**) and open phase 2019 (**b**). Estimated flux potential is shaded in blue where the upper bound is associated with difference in PCO_2 from the A_T-salinity$_{in\ situ}$ regression, and the lower bound associated with freshwater Schmidt number. The upper and lower bounds for open 2018 were 10.67 and 2.23 μmol C m^{-2} min^{-1} while open 2019 upper and lower bounds were 8.56 and 5.52 μmol C m^{-2} min^{-1}, respectively.